

## Nonparaxial propagation of ultrashort laser pulses in plasma channels

E. Esarey and W. P. Leemans

Center for Beam Physics, Ernest Orlando Lawrence Berkeley National Laboratory,  
University of California, Berkeley, California 94720

(Received 28 May 1998)

The propagation characteristics of an ultrashort laser pulse in a preformed plasma channel are analyzed. The plasma channel is assumed to be parabolic and unperturbed by the laser pulse. Solutions to the wave equation beyond the paraxial approximation are derived that include finite pulse length effects and group velocity dispersion. When the laser pulse is mismatched within the channel, betatron oscillations arise in the laser pulse envelope. A finite pulse length leads to a spread in the laser wave number and consequently a spread in betatron wave number. This results in phase mixing and damping of the betatron oscillation. The damping distance characterizing the phase mixing of the betatron oscillation is derived, as is the dispersion distance characterizing the longitudinal spreading of the pulse. [S1063-651X(99)04301-9]

PACS number(s): 52.40.Nk, 52.40.Fd, 42.79.Gn, 42.65.Re

### I. INTRODUCTION

Optical guiding of intense laser pulses in plasma channels [1] is beneficial to a variety of applications, including plasma-based accelerators [2], harmonics generation [3,4], x-ray lasers [5,6], and advanced laser-fusion schemes [7–9]. In vacuum, a laser pulse will diffractively expand after a distance on the order of a Rayleigh length  $Z_R = \pi r_0^2 / \lambda$ , where  $r_0$  is the laser spot radius at focus,  $\lambda = 2\pi c / \omega_0$  is the laser wavelength, and  $\omega_0$  is the laser frequency. High intensity requires a tight focus (small  $r_0$ ) and, hence, a small Rayleigh length, e.g.,  $Z_R \approx 300 \mu\text{m}$  for  $r_0 = 10 \mu\text{m}$  and  $\lambda = 1 \mu\text{m}$ . A preformed plasma density channel can prevent pulse diffraction. Specifically, a plasma channel with a radially parabolic density profile of the form  $n(r) = n_0 + \Delta n r^2 / r_0^2$  can guide a laser pulse of spot size  $r_0$  provided the channel depth  $\Delta n$  satisfies  $\Delta n = \Delta n_c$ , where  $\Delta n_c = 1 / \pi r_e r_0^2$  is the critical channel depth and  $r_e = e^2 / m_e c^2$  is the classical electron radius [10,11]. In practical units,

$$\Delta n_c (\text{cm}^{-3}) \approx 1.13 \times 10^{20} / r_0^2 (\mu\text{m}), \quad (1)$$

e.g.,  $\Delta n \approx 10^{18} \text{cm}^{-3}$  for  $r_0 = 10 \mu\text{m}$ . Plasma density channels have been created in the laboratory by a variety of methods: (i) Passing a long laser pulse through an optic to create a line focus in a gas, which ionizes and heats the gas, creating a radially expanding hydrodynamic shock [12–18], (ii) using a slow capillary discharge to control the plasma profile [19–21], and (iii) using the ponderomotive force of an intense, relativistically self-guided laser pulse in a plasma, which creates a channel in its wake [22–31]. These methods have been used to guide short pulses, with intensities as high as  $10^{16} \text{W/cm}^2$ , over distances on the order of  $20 Z_R - 100 Z_R$  [12–24]. In all experiments published to date [12–24], the laser pulses guided within the preformed plasma channels were in the regime  $a_0^2 \ll 1$  and  $P/P_c \ll 1$ , where  $a_0^2 = 7.2 \times 10^{-19} \lambda^2 (\mu\text{m}) I (\text{W/cm}^2)$ ,  $I$  is the laser intensity,  $P (\text{GW}) = 21.5 (a_0 r_0 / \lambda)^2$  is the laser power,  $P_c (\text{GW}) = 17 (\lambda_p / \lambda)^2$  is the critical power for relativistic self-focusing,  $\lambda_p = 2\pi c / \omega_{p0}$  is the plasma wavelength, and  $\omega_{p0} = (4\pi n_0 e^2 / m_e)^{1/2}$  is the electron plasma frequency.

In this paper, the propagation of ultrashort pulses in long plasma channels is examined in the low intensity  $a_0^2 \ll 1$ , low power  $P/P_c \ll 1$  limits. Solutions to the linear wave equation are derived beyond the paraxial limit, i.e., finite pulse length and group velocity dispersion effects are retained. A formalism is developed that allows the laser field profile to be calculated in three dimensions to arbitrarily high order in the parameter  $\lambda/L$ . It is found that betatron oscillations in the laser pulse envelope, which occur when the pulse is not matched within the channel, damp due to phase mixing with a characteristic damping length given by  $Z_\beta \approx (\pi L / \lambda) Z_R = (\pi r_0 / \lambda)^2 L$ . In addition, the characteristic scale length for dispersive spreading of the laser pulse length within a channel is found to be given by  $Z_D \approx (\gamma_g L / r_0)^2 Z_R$ , where  $\gamma_g = (1 - \beta_g^2)^{-1/2}$  and  $v_g = c \beta_g$  is the group velocity of the laser pulse within the channel, i.e.,  $\beta_g \approx 1 - \omega_{p0}^2 / 2\omega^2 - 2c^2 / \omega_0^2 r_0^2$ , assuming  $1 - \beta_g \ll 1$ . These effects are important for ultrashort laser pulses, and high-power ( $\geq 1 \text{ TW}$ ) sources of ultrashort ( $\leq 20 \text{ fs}$ ) pulses are readily available [32].

Solutions to the paraxial wave equation describing the propagation of laser pulses in underdense ( $\omega_0 \gg \omega_{p0}$ ) plasma channels have been analyzed in detail [1]. Analysis of the paraxial wave equation with a parabolic density channel of the form  $n(r) = n_0 + \Delta n r^2 / r_0^2$  indicates that the normalized spot size  $R = r_s / r_0$  of a long, axially uniform laser beam evolves via [1,33]

$$\frac{d^2 R}{dz^2} = \frac{1}{Z_R^2 R^3} \left( 1 - \frac{P}{P_c} - \frac{\Delta n}{\Delta n_c} R^4 \right), \quad (2)$$

where  $Z_R = \pi r_0^2 / \lambda$ ,  $\Delta n_c = 1 / \pi r_e r_0^2$  is the critical channel depth,  $P$  is the laser power, and  $P_c \approx 17 (\lambda_p^2 / \lambda^2) \text{ GW}$  is the critical power for relativistic self-focusing [1,34–38]. Note that  $P_c \approx 19 \text{ TW}$  for  $n_0 \approx 10^{18} \text{cm}^{-3}$  ( $\lambda_p \approx 33 \mu\text{m}$ ) and  $\lambda = 1 \mu\text{m}$ . The first, second, and third terms on the right of Eq. (2) represent the effects of vacuum diffraction, relativistic self-focusing, and channel focusing, respectively. In deriving Eq. (2), a Gaussian radial laser field profile was assumed, i.e., a normalized laser intensity profile of the form

$$|a|^2 = a_0^2 (r_0^2/r_s^2) \exp(-2r^2/r_s^2), \quad (3)$$

where  $\mathbf{a} = e\mathbf{A}/m_e c^2$  is the normalized vector potential. The parameter  $a_0$  is related to the laser power and peak intensity  $I$  at the focal spot  $r_s = r_0$  by  $a_0^2 = 7.2 \times 10^{-19} \lambda^2 (\mu\text{m}) I (\text{W}/\text{cm}^2)$  and  $P (\text{GW}) = 21.5 (a_0^2 r_0^2 / \lambda^2)$ , assuming linear polarization. Furthermore, the derivation of Eq. (2) assumes a long laser pulse  $L \gg \lambda_p$  and neglects ponderomotive and wake-field effects [1,10,11,33,35,37,38], i.e., the parabolic density profile is assumed to be unaffected by the laser pulse. Other channel profiles, e.g., square or hollow channels [39,40], are not considered in this paper. In the limits  $\Delta n/\Delta n_c \ll 1$  and  $P/P_c \ll 1$ , the usual solution for vacuum diffraction is recovered from Eq. (2), i.e.,  $r_s = r_0(1 + z^2/Z_R^2)^{1/2}$ , assuming the initial conditions  $r_s = r_0$  and  $dr_s/dz = 0$  at  $z = 0$ .

Equation (2) indicates that the condition for matched-beam propagation (propagation with a constant spot size  $r_s = r_0$ ) is [1,33,38]

$$\Delta n/\Delta n_c = 1 - P/P_c. \quad (4)$$

In the absence of a channel, guiding requires  $P = P_c$ , which is the condition of relativistic self-guiding. As is discussed in detail in Refs. [1, 11, 33, 36], relativistic self-guiding is subject to leading-edge erosion and self-modulation instabilities, and is ineffective in preventing the diffraction of short pulses, i.e., pulse lengths  $L \leq \lambda_p$ . For low powers,  $P \ll P_c$ , matched-beam propagation can be achieved by a channel with  $\Delta n = \Delta n_c$ . Matched-beam propagation requires, in addition to Eq. (4), that the beam be injected into the channel with a spot size  $r_s$  satisfying  $dr_s/dz = 0$  and  $r_s = r_0$  at the channel entrance, where the  $z$  axis corresponds to the channel axis.

In general, the beam will not be perfectly matched within the channel, i.e., the laser envelope will undergo betatron oscillations. The solution to Eq. (2) for the initial ( $z = 0$ ) conditions  $dr_s/dz = 0$  and  $r_s = r_i$  is [1,33]

$$\frac{r_s^2}{r_i^2} = \frac{\Delta n_c r_0^4}{2\Delta n r_i^4} \left[ 1 - \frac{P}{P_c} + \frac{\Delta n r_i^4}{\Delta n_c r_0^4} - \left( 1 - \frac{P}{P_c} - \frac{\Delta n r_i^4}{\Delta n_c r_0^4} \right) \cos(k_\beta z) \right], \quad (5)$$

where  $k_\beta = (2/Z_R)(\Delta n/\Delta n_c)^{1/2}$  is the betatron wave number and  $r_i$  is the injected spot size. For  $P < P_c$  and  $\Delta n > 0$ , the spot size oscillates between  $r_s^2 = r_i^2$  and  $r_s^2 = (1 - P/P_c)\Delta n_c r_0^4/\Delta n r_i^2$  with an oscillation period  $\lambda_\beta = 2\pi/k_\beta = \pi Z_R(\Delta n_c/\Delta n)^{1/2}$ . A matched beam with  $r_s = r_i = r_0$  requires  $P = P_M$ , where  $P_M = P_c(1 - \Delta n/\Delta n_c)$ . Notice that for  $r_i = r_0$  and  $k_\beta^2 z^2 \ll 1$ , Eq. (5) reduces to  $r_s^2/r_0^2 = 1 + (1 - P/P_c - \Delta n/\Delta n_c)z^2/Z_R^2$ . This indicates that the beam will initially focus for  $P > P_M$  or diffract for  $P < P_M$  with an effective Rayleigh length of  $Z_R(1 - P/P_c - \Delta n/\Delta n_c)^{-1/2}$ .

Equations (2)–(5) are solutions to the paraxial wave equation describing the evolution of long laser beams. However, some effects of a finite pulse length  $L$  can be ascertained from Eqs. (2)–(5) in the limit  $P/P_c \ll 1$ . A finite pulse length

will introduce a spread in laser wave numbers  $k = k_0 + \delta k$ , where  $k_0$  is the central wave number and  $|\delta k| \approx 2/L \ll k_0$ . Notice that the condition for guiding a matched pulse with  $r_i = r_0$  is  $\Delta n = \Delta n_c$ , which is independent of the wave number. For a slight mismatch,  $r_i = r_0 + \delta r_0$  with  $\delta r_0/r_0 \ll 1$ , the solution to Eq. (2) is  $r_s \approx r_0 + \delta r_0 \cos k_\beta z$ . Notice that the betatron wave number  $k_\beta = 2/Z_R = 4/k r_0^2$  depends on the  $k$  spectrum of the laser pulse. A spread in  $k$  will lead to a spread in  $k_\beta$ , i.e., different frequencies will undergo betatron oscillations in the channel with different periods. This will lead to phase-mixing and damping of the betatron oscillations. Roughly, damping of the betatron oscillations will occur after a distance  $Z_\beta$  given by  $\delta k_\beta Z_\beta \approx \pi/2$ , where  $\delta k_\beta = k_\beta \delta k/k_0$ . This gives  $Z_\beta \approx (\pi/8)k_0 L Z_R$ . A more accurate estimate is given by averaging the betatron orbit  $\delta r = \delta r_0 \cos k_\beta z$  over the  $k$  spectrum. A laser pulse with an axial profile of the form  $a \sim \exp[-(z-ct)^2/L^2]$  has a  $k$  spectrum  $f \sim \exp(-\delta k^2 L^2/4)$ . Hence,  $\langle \delta r \rangle = \int d\delta k f \delta r \approx \delta r_0 \cos(k_{\beta 0} z) \exp(-k_{\beta 0}^2 z^2/k_0^2 L^2)$ , which implies  $Z_\beta = k_0 L/k_{\beta 0} = k_0 L Z_{R0}/2$ , where  $Z_{R0} = k_0 r_0^2/2$ . This result holds provided  $L < Z_R$ . Damping of the betatron oscillations in the laser spot has been observed in nonlinear fluid simulations that model the experiments of Ref. [21].

The remainder of this paper is organized as follows. Section II presents an analysis of the linear wave equation including finite pulse length and group velocity dispersion effects. Solutions for a matched, finite length pulse within a channel, including second-order dispersion, are derived in Sec. III. In Sec. IV, mismatched pulse propagation is analyzed, with (Sec. IV A) and without (Sec. IV B) the effects of dispersion. Nonlinear effects, in particular the hose-modulation instability, are discussed in Sec. V. Section VI presents a discussion of the results. Three Appendixes are also included that discuss the plasma source term for the linear wave equation (Appendix A), the evolution of ultrashort laser pulses in the absence of a plasma channel (Appendix B), and a generalization of the results to include high-order modes (Appendix C).

## II. ANALYSIS OF WAVE EQUATION

The propagation of an ultrashort laser pulse in a preformed plasma channel will be considered. A parabolic density channel is assumed with an electron density profile of the form  $n(r) = n_0 + \Delta n r^2/r_0^2$ , where  $\Delta n$  is the channel depth and  $r_0$  is the channel radius. Propagation is considered in the limits of low power  $P/P_c \ll 1$  and low intensity  $a_0^2 \ll 1$ , such that nonlinear effects (e.g., relativistic self-focusing) can be neglected and the density channel can be assumed unaffected by the laser pulse. It is convenient to use the normalized vector potential  $\mathbf{a} = e\mathbf{A}/m_e c^2$  with  $\nabla \cdot \mathbf{a} = 0$ . The linear wave equation for the transverse component  $a_x$  of the laser field is

$$\left( \nabla^2 - \frac{1}{c^2} \frac{\partial^2}{\partial t^2} \right) a_x = k_p^2(r) a_x, \quad (6)$$

where  $k_p^2(r) = k_{p0}^2(1 + \Delta n r^2/n_0 r_0^2)$ ,  $k_{p0} = \omega_{p0}/c$ , and  $\omega_{p0}^2 = 4\pi n_0 e^2/m_e$ . Here, the source term  $S_x = k_p^2(r) a_x$  represents the normalized transverse plasma current to first order

in  $|a_x|$ . Derivation of the plasma source term, along with high-order corrections, is discussed in Appendix A.

In terms of the independent variables  $\zeta = z - \beta_{g0}ct$  and  $z$ , the wave equation becomes

$$\left[ \nabla_{\perp}^2 + 2 \frac{\partial^2}{\partial \zeta \partial z} + (1 - \beta_{g0}^2) \frac{\partial^2}{\partial \zeta^2} + \frac{\partial^2}{\partial z^2} \right] a_x = k_p^2(r) a_x, \quad (7)$$

where  $\beta_{g0} = v_{g0}/c$  and  $v_{g0}$  is the linear pulse group velocity, as is defined below. Introducing the slowly varying field envelope  $\hat{a}$ , where  $a_x = \hat{a} \exp(ik_0z - i\omega_0t) + \text{c.c.}$ ,  $\omega_0$  is the central frequency of the pulse,  $k_0$  is the central wave number, and c.c. denotes the complex conjugate, the wave equation becomes

$$\left[ \nabla_{\perp}^2 + 2 \left( ik_0 + \frac{\partial}{\partial \zeta} \right) \frac{\partial}{\partial z} + (1 - \beta_{g0}^2) \frac{\partial^2}{\partial \zeta^2} + \frac{\partial^2}{\partial z^2} \right] \hat{a} = [k_p^2(r) - k_0^2(\beta_{p0}^2 - 1)] \hat{a}, \quad (8)$$

where  $\beta_{p0} = \omega_0/c k_0$  and  $\beta_{p0}\beta_{g0} = 1$  is assumed.

For a short pulse of length  $L$  propagating in a plasma channel, the operators on the left side of the wave equation, Eq. (8), scale as follows:  $\nabla_{\perp}^2 \sim 1/r_0^2$ ,  $\partial/\partial \zeta \sim 1/L$ ,  $\partial/\partial z \sim 1/Z_{R0}$ , and  $1 - \beta_{g0}^2 \sim \omega_{p0}^2/\omega_0^2 + 4/k_0^2 r_0^2$ , where  $Z_{R0} = k_0 r_0^2/2$  is the Rayleigh length. The last term on the left of Eq. (8),  $\partial^2/\partial z^2$ , is typically small and will be neglected in the following analysis. This is valid provided (i)  $|\partial^2 \hat{a}/\partial z^2| \ll 2|\partial^2 \hat{a}/\partial \zeta \partial z|$ , which implies  $L \ll 2Z_{R0}$ , and (ii)  $|\partial^2 \hat{a}/\partial z^2| \ll (1 - \beta_{g0}^2)|\partial^2 \hat{a}/\partial \zeta^2|$ , which implies  $L^2/r_0^2 \ll (1 + k_{p0}^2 r_0^2/4)$ . The  $2\partial^2/\partial \zeta \partial z$  and  $(1 - \beta_{g0}^2)\partial^2/\partial \zeta^2$  terms in Eq. (8) represent corrections to the paraxial wave equation that account for short pulse and group velocity dispersion effects.

Equation (8) can be solved by taking a Fourier transform with respect to  $\zeta$  [41]. Neglecting the  $\partial^2/\partial z^2$  term gives

$$\left[ \nabla_{\perp}^2 + 2i(k_0 + \delta k) \frac{\partial}{\partial z} \right] \hat{a}_k = [k_p^2(r) - k_0^2(\beta_{p0}^2 - 1) + \delta k^2(1 - \beta_{g0}^2)] \hat{a}_k, \quad (9)$$

where

$$\hat{a}_k = \frac{1}{\sqrt{2\pi}} \int_{-\infty}^{\infty} d\zeta \exp(-i\delta k\zeta) \hat{a}(\zeta). \quad (10)$$

Notice that Eq. (9) has the form of a paraxial wave equation. Hence, solutions for  $\hat{a}_k$  can readily be found. For example, the lowest-order Gaussian mode is given by

$$\hat{a}_k = b_k \exp[i\theta - (1 - i\alpha)r^2/r_s^2], \quad (11)$$

where the quantities  $b_k(k, z)$ ,  $\theta(k, z)$ ,  $\alpha(k, z)$ , and  $r_s(k, z)$ , which represent the amplitude, phase shift, curvature, and spot size of the field in  $k$  space, respectively, satisfy

$$b_k = b_{k0} r_s / r_0, \quad (12a)$$

$$\alpha = (kr_s/2) \partial r_s / \partial z, \quad (12b)$$

$$\frac{\partial^2 r_s}{\partial z^2} = \frac{4}{k^2 r_s^3} \left( 1 - \frac{\Delta n r_s^4}{\Delta n_c r_0^4} \right), \quad (12c)$$

$$\frac{\partial \theta}{\partial z} = -\frac{2}{k} \left( \frac{1}{r_s^2} - \frac{1}{r_0^2} \right) - \frac{\delta k^2}{2k} (1 - \beta_{g0}^2), \quad (12d)$$

where  $k = k_0 + \delta k$ ,  $\Delta n_c = 1/\pi r_e r_0^2$  is the critical channel depth, and  $b_{k0}$  is the initial  $k$  spectrum of the laser pulse at  $z=0$ . Note that for an initial Gaussian axial pulse profile of the form  $b_0 = a_0 \exp(-\zeta^2/L^2)$ ,  $b_{k0} = a_0(L/\sqrt{2}) \exp(-\delta k^2 L^2/4)$ . In deriving Eq. (12d), the central pulse frequency and wave number are assumed to satisfy

$$\omega_0^2/c^2 - k_0^2 = k_{p0}^2 + 4/r_0^2, \quad (13)$$

which implies

$$\beta_{g0}^2 = \beta_{p0}^{-2} = 1 - \omega_{p0}^2/\omega_0^2 - 4c^2/\omega_0^2 r_0^2. \quad (14)$$

This is the correct group velocity for a Gaussian laser pulse propagating at the matched spot size  $r_s = r_0$  in a channel with  $\Delta n = \Delta n_c$ , as demonstrated in Sec. III. Furthermore, note that in the limit of a long laser beam, Eqs. (12a)–(12d) reduce to the usual paraxial solutions when  $\delta k = 0$ .

Equation (12c) describes the evolution of the spot size  $r_s(z)$  for a given  $k = k_0 + \delta k$  mode of the laser field. For a given  $k$ ,  $r_s$  undergoes ‘‘betatron’’ oscillations in the density channel. For example, the solutions to Eqs. (12b)–(12d) with the initial (at  $z=0$ ) conditions  $\alpha=0$ ,  $\theta=0$ ,  $\partial r_s/\partial z=0$ , and  $r_s = r_i$  are given by

$$\alpha = -\frac{1}{2} \left( \frac{r_i^2}{r_M^2} - \frac{r_M^2}{r_i^2} \right) \sin(k\beta z), \quad (15a)$$

$$r_s^2 = \frac{r_i^2}{2} \left[ \left( 1 + \frac{r_M^4}{r_i^4} \right) + \left( 1 - \frac{r_M^4}{r_i^4} \right) \cos(k\beta z) \right], \quad (15b)$$

$$\theta = \left[ \frac{r_M^2}{r_0^2} - \frac{\delta k^2 r_M^2}{4} (1 - \beta_{g0}^2) \right] \frac{z}{Z_{RM}} - \tan^{-1} \left[ \frac{r_M^2}{r_i^2} \tan \left( \frac{z}{Z_{RM}} \right) \right], \quad (15c)$$

where  $k\beta = 2/Z_{RM}$  is the betatron wave number,  $Z_{RM} = k r_M^2/2$  is the matched Rayleigh length, and  $r_M = (r_0^4 \Delta n_c / \Delta n)^{1/4}$  is the matched spot size ( $r_M = r_0$  for  $\Delta n = \Delta n_c$ ). The normalized spot size  $r_s/r_0$  in the paraxial limit, i.e., obtained from Eq. (15b) with  $\delta k = 0$  and  $\Delta n = \Delta n_c$ , is plotted in Fig. 1 versus  $z/Z_R$  for the matched case  $r_i = r_0$  (solid curve), and two mismatched cases:  $r_i = 1.5r_0$  (dashed curve) and  $r_i = 0.5r_0$  (dotted curve).

The solution for the laser envelope is given by

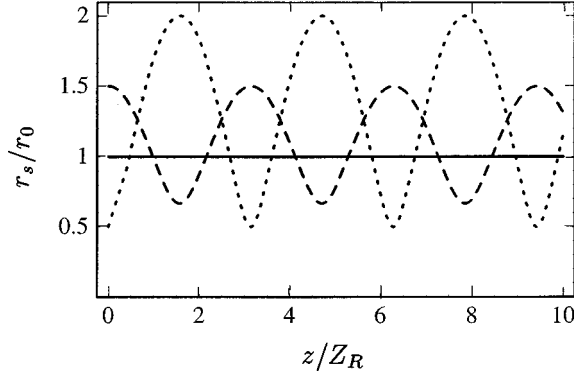


FIG. 1. Normalized spot size  $r_s/r_0$  in the paraxial limit ( $\delta k = 0$ ), Eq. (15b), vs  $z/Z_R$  for  $r_i = r_0$  (solid curve),  $r_i = 1.5r_0$  (dashed curve), and  $r_i = 0.5r_0$  (dotted curve), with  $\Delta n = \Delta n_c$ .

$$\hat{a}(r, \zeta, z) = \frac{1}{\sqrt{2\pi}} \int_{-\infty}^{\infty} d\delta k \frac{r_0}{r_s} b_{k_0} \times \exp \left[ i\delta k \zeta + i\theta - (1 - i\alpha) \frac{r^2}{r_s^2} \right], \quad (16)$$

where  $\alpha(k, z)$ ,  $r_s(k, z)$ , and  $\theta(k, z)$  are given by Eqs. (15a)–(15c), and  $b_{0k}$  is the Fourier transform of the initial ( $z=0$ ) axial profile of the laser pulse  $b_0(\zeta)$ . Strictly speaking,  $b_{0k}$  should not contain a finite amplitude at  $\delta k = -k_0$  [41], so as to avoid singularities that may arise in the integrand of Eq. (16). Note that a finite component at  $\delta k = -k_0$  ( $k=0$ ) corresponds to a contribution to the field envelope  $\hat{a}$  that is spatially uniform in  $z$ . An axially uniform contribution to the field envelope is not physical for a realistic ultrashort laser pulse. Approximate solutions to Eq. (16) can be found by expanding the integrand for  $|\delta k|/k_0 \ll 1$  [41]. Solutions to Eqs. (11)–(12) and (16) for the case of vacuum diffraction ( $\Delta n = 0$ ) are discussed in Appendix B. Generalization of Eqs. (11)–(16) to describe high-order Laguerre-Gaussian modes is discussed in Appendix C.

Notice that the condition for a matched beam,  $r_s = r_0$  for  $\Delta n = \Delta n_c$ , is independent of wave number  $k$ , since  $\Delta n_c$  is independent of  $k$ . The betatron wave number, however, does depend on  $k$ , i.e.,  $k_\beta = 4/kr_M^2$ . Hence, for a short pulse, the spread in  $k$  implies a spread in  $k_\beta$  which leads to phase mixing and a subsequent damping of the betatron oscillations.

### III. MATCHED PULSE

Since the condition for guiding a pulse with a constant radius  $r_s = r_0$  for  $\Delta n = \Delta n_c$  is independent of wave number, matched pulse solutions are possible. Consider a matched pulse with  $\Delta n = \Delta n_c$  and  $r_s = r_0$ . Equations (12)–(15) imply  $b_k = b_{k_0}$ ,  $\alpha = 0$ , and  $\theta = -(\delta k^2/2k)(1 - \beta_{g0}^2)z$ . Hence,

$$\hat{a}_k = b_{k_0} \exp[-r^2/r_0^2 - (\delta k^2/2k)(1 - \beta_{g0}^2)z]. \quad (17)$$

Here, the last term on the right, proportional to  $\delta k^2 z/k$ , represents the effects of group velocity dispersion. For a Gaussian axial pulse profile,  $b_{k_0} = a_0(L/\sqrt{2})\exp(-\delta k^2 L^2/4)$  and  $|\delta k| \sim 1/L \ll k_0$ . Hence, in the dispersion term the ap-

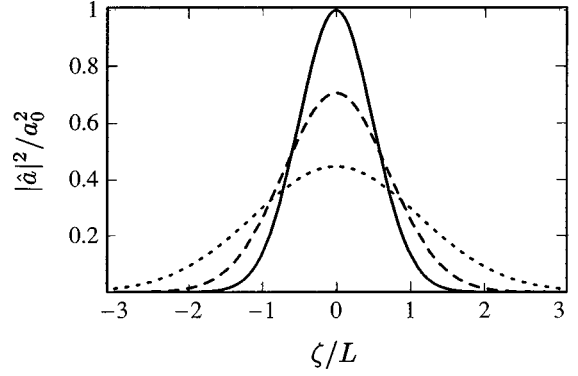


FIG. 2. Normalized intensity  $|\hat{a}|^2/a_0^2$ , Eq. (21), vs  $\zeta/L$  along the axial axis ( $r=0$ ) for a matched pulse at  $z=0$  (solid curve),  $z=Z_{D0}$  (dashed curve), and  $z=2Z_{D0}$  (dotted curve).

proximation  $\delta k^2 z/k \approx \delta k^2 z/k_0$  can be made (i.e., only second-order dispersion effects are retained). Using this approximation, and assuming a Gaussian axial profile, the Fourier inverse transform of Eq. (17) is given by

$$\hat{a} = a_0(1 + \eta_0^2)^{-1/4} \times \exp \left[ -\frac{r^2}{r_0^2} - \frac{\zeta^2}{L^2} \frac{(1 - i\eta_0)}{(1 + \eta_0^2)} - \frac{i}{2} \tan^{-1} \eta_0 \right], \quad (18)$$

where  $\eta_0 = z/Z_{D0}$  and

$$Z_{D0} = \frac{k_0 L^2}{2(1 - \beta_{g0}^2)} = \frac{(\pi L/\lambda_0)^2 Z_{R0}}{(1 + k_{p0}^2 r_0^2/4)} \quad (19)$$

is the dispersion length, where  $\lambda_0 = 2\pi c/\omega_0$ . Dispersion causes a broadening of the pulse length, i.e., the effective pulse length is given by

$$L_{e0} = L(1 + z^2/Z_{D0}^2)^{1/2}. \quad (20)$$

The normalized pulse intensity is given by

$$|\hat{a}|^2 = a_0^2 (L/L_{e0}) \exp(-2r^2/r_0^2 - 2\zeta^2/L_{e0}^2). \quad (21)$$

The normalized intensity  $|\hat{a}|^2/a_0^2$  versus  $\zeta/L$  is plotted in Fig. 2 along the  $z$  axis ( $r=0$ ) for  $z=0$  (solid curve),  $z=Z_{D0}$  (dashed curve), and  $z=2Z_{D0}$  (dotted curve). Notice that the axial pulse centroid, corresponding to the position of the peak intensity, is given by  $\zeta=0$ . Hence, the group velocity of the pulse centroid  $v_{g\zeta}$  is correctly given by  $v_{g\zeta}^2/c^2 = \beta_{g0}^2 = 1 - \omega_{p0}^2/\omega_0^2 - 4c^2/\omega_0^2 r_0^2$ .

### IV. MISMATCHED PULSE

Consider the case of a pulse injected into a channel  $\Delta n = \Delta n_c$  with a slightly mismatched radius, i.e.,  $dr_s/dz = 0$  and  $r_s = r_0 + \delta r_0$  at  $z=0$  with  $\delta r_0^2/r_0^2 \ll 1$ . To leading order in  $\delta r_0/r_0$ , Eqs. (12) and (15) indicate

$$\alpha \approx -2 \frac{\delta r_0}{r_0} \sin(k_\beta z), \quad (22a)$$

$$r_s \approx r_0 \left[ 1 + \frac{\delta r_0}{r_0} \cos(k_\beta z) \right], \quad (22b)$$

$$b_k \approx b_{k_0} \left[ 1 - \frac{\delta r_0}{r_0} \cos(k_\beta z) \right], \quad (22c)$$

$$\theta \approx \frac{\delta r_0}{r_0} \sin(k_\beta z) - \frac{\delta k^2}{2k} (1 - \beta_{g0}^2) z. \quad (22d)$$

Thus, to leading order in  $\delta r_0/r_0$ ,

$$\begin{aligned} \hat{a}_k \approx & b_{k_0} \left[ 1 - \frac{\delta r_0}{r_0} \left( 1 - \frac{2r^2}{r_0^2} \right) \exp(-ik_\beta z) \right] \\ & \times \exp \left[ -\frac{r^2}{r_0^2} - \frac{i\delta k^2}{2k} (1 - \beta_{g0}^2) z \right]. \end{aligned} \quad (23)$$

This can be written as  $\hat{a}_k = \hat{a}_{k_0} + \delta \hat{a}_k$ , where  $\hat{a}_{k_0}$  is the matched fundamental ( $m=0$  and  $p=0$ ) mode and  $\delta \hat{a}_k$  (the term proportional to  $\delta r_0/r_0$ ) is the matched first-order ( $m=1$  and  $p=0$ ) Laguerre-Gaussian mode, as discussed in Appendix C.

### A. No dispersion

First consider the limit in which second-order group velocity dispersion effects are neglected, i.e., the term proportional to  $\delta k^2 z/k$  is neglected in the exponent of Eq. (23). To evaluate Eq. (23),  $k_\beta$  is expanded to first order in  $|\delta k|/k_0$ , assuming  $\delta k^2/k_0^2 \ll 1$ , i.e.,  $k_\beta \approx k_{\beta 0}(1 - \delta k/k_0)$ , where  $k_{\beta 0} = 2/Z_{R0}$  and  $Z_{R0} = k_0 r_0^2/2$ . The Fourier inverse transform of Eq. (23), including terms in the exponent to first order in  $\delta k/k_0$ , is given by  $\hat{a} = \hat{a}_0 + \delta \hat{a}$ , where

$$\hat{a}_0 = b_0(\zeta) \exp(-r^2/r_0^2) \quad (24)$$

is the matched pulse solution in the absence of second-order group velocity dispersion, e.g., given by Eq. (18) in the limit  $Z_{D0}^{-1} = 0$ . The perturbation to the pulse envelope due to the mismatch is given by

$$\delta \hat{a} = -\frac{\delta r_0}{r_0} b_0(\zeta_1) \left( 1 - \frac{2r^2}{r_0^2} \right) \exp \left( -\frac{r^2}{r_0^2} - ik_{\beta 0} z \right), \quad (25)$$

where  $\zeta_1 = \zeta + k_{\beta 0} z/k_0$ . Here,  $b_0(\zeta)$  is the initial axial field profile, which for a Gaussian is given by  $b_0(\zeta) = a_0 \exp(-\zeta^2/L^2)$ . The fundamental field  $\hat{a}_0$ , Eq. (24), and the normalized perturbed field  $\hat{a}_1 = \delta \hat{a}/(\delta r_0/r_0)$ , given by Eq. (25), versus  $\zeta/L$  and  $r/r_0$  are shown in Figs. 3(a) and 3(b), respectively, at  $z = 5\pi Z_{R0}$  for a Gaussian axial profile with  $L/\lambda_0 = 5$ . In Fig. 3, note that the centroid of the perturbed field lags behind the fundamental by an amount  $\Delta \zeta/L = -k_{\beta 0} z/k_0 L = -1$ .

The centroid of the perturbed field  $\delta \hat{a}$  (given by  $\zeta_1 = 0$ ) is shifted behind that of the unperturbed field  $\hat{a}_0$  (given by  $\zeta = 0$ ) by an amount  $\Delta \zeta = \zeta - \zeta_1 = -k_{\beta 0} z/k_0$ . This indicates that the group velocity  $v_{g1} = c\beta_{g1}$  associated with the centroid of the perturbed field is given by

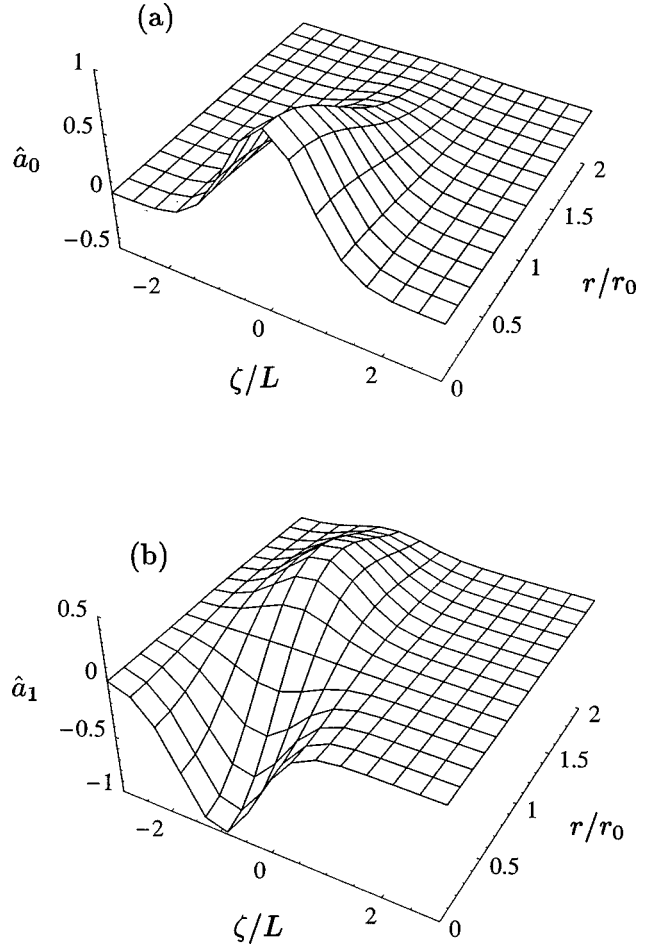


FIG. 3. Surface plots of (a) fundamental field  $\hat{a}_0$ , Eq. (24), and (b) normalized perturbed field  $\hat{a}_1 = \delta \hat{a}/(\delta r_0/r_0)$ , given by Eq. (25), vs  $\zeta/L$  and  $r/r_0$  at  $z = 5\pi Z_{R0}$  for a Gaussian axial profile with  $L/\lambda_0 = 5$ .

$$\beta_{g1} = \beta_{g0}(1 + k_{\beta 0}/k_0)^{-1} \approx 1 - \omega_{p0}^2/2\omega_0^2 - 6c^2/\omega_0^2 r_0^2, \quad (26)$$

which is less than that of the unperturbed field by an amount  $\beta_{g0} - \beta_{g1} \approx 4/k_0^2 r_0^2$ , where  $\omega_{p0}^2/\omega_0^2 \ll 1$  and  $c^2/\omega_0^2 r_0^2 \ll 1$  have been assumed. The perturbed field, Eq. (25), can be interpreted as a matched first-order ( $m=1, p=0$ ) Laguerre-Gaussian mode in the absence of dispersion (see Appendix C). The effective axial wave-number shift  $\delta k_z$  associated with a Laguerre-Gaussian mode is given by  $\delta k_z/k_0 \approx -2(2m+p+1)c^2/\omega_0^2 r_0^2$ , which is agreement with the third term on the left of Eq. (14) for ( $m=0, p=0$ ) and of Eq. (26) for ( $m=1, p=0$ ).

To analyze the behavior of the pulse radius, consider the *local* intensity-weighted mean-squared radius  $\langle r^2 \rangle$  defined by

$$\langle r^2 \rangle = \frac{\int_0^\infty dr r^3 |\hat{a}|^2}{\int_0^\infty dr r |\hat{a}|^2}. \quad (27)$$

To first order in  $\delta r_0/r_0$ , the normalized pulse intensity is given by  $|\hat{a}|^2 = \hat{I}_0 + \delta \hat{I}$  with  $\hat{I}_0 = |\hat{a}_0|^2 = b_0^2(\zeta) \exp(-2r^2/r_0^2)$  and  $\delta \hat{I} = \hat{a}_0 \delta \hat{a}^* + \hat{a}_0^* \delta \hat{a}$ , where the asterisk signifies the complex conjugate, i.e.,

$$\delta \hat{l} = -2b_0(\zeta)b_0(\zeta_1) \frac{\delta r_0}{r_0} \left(1 - \frac{2r^2}{r_0^2}\right) \times \exp\left(-\frac{2r^2}{r_0^2}\right) \cos(k_{\beta 0}z). \quad (28)$$

Hence, to first order in  $\delta r_0/r_0$ ,

$$\int_0^\infty dr r |\hat{a}|^2 = \frac{r_0^2}{4} b_0^2(\zeta), \quad (29)$$

which indicates that the perturbation does not alter the pulse power. Furthermore,

$$\langle r^2 \rangle = \frac{r_0^2}{2} \left[ 1 + 2 \frac{\delta r_0}{r_0} \frac{b_0(\zeta_1)}{b_0(\zeta)} \cos(k_{\beta 0}z) \right], \quad (30)$$

which for a Gaussian axial profile,  $b_0(\zeta) = a_0 \exp(-\zeta^2/L^2)$ , gives

$$\langle r^2 \rangle = \frac{r_0^2}{2} \left[ 1 + 2 \frac{\delta r_0}{r_0} \Delta R_L(\zeta, z) \right], \quad (31)$$

where

$$\Delta R_L = \exp\left(-\frac{2z\zeta}{Z_\beta L} - \frac{z^2}{Z_\beta^2}\right) \cos(k_{\beta 0}z) \quad (32)$$

is the normalized local intensity-weighted RMS betatron radius. Asymptotically, for a fixed  $\zeta$  and  $z \gg Z_\beta$ , the betatron oscillation damps via  $\exp(-z^2/Z_\beta^2)$ , where

$$Z_\beta = (k_0 L/2) Z_{R0} \approx (\pi L/\lambda_0) Z_{R0} \quad (33)$$

is the betatron damping distance. Furthermore, note that there is a front-to-back asymmetry in the betatron oscillation, i.e., the magnitude of the betatron oscillation at the front of the pulse ( $\zeta = L/2$ ) is smaller than it is at the back of the pulse ( $\zeta = -L/2$ ). The normalized local RMS radius of the betatron oscillation  $\Delta R_L(\zeta, z)$ , Eq. (32), is plotted in Figs. 4(a) and 4(b) versus  $z/Z_{R0}$  for the parameters  $\lambda_0 = 1 \mu\text{m}$ ,  $L = 5 \mu\text{m}$ , and  $r_0 = 10 \mu\text{m}$  ( $Z_\beta = 5\pi Z_{R0}$  and  $Z_{R0} = 310 \mu\text{m}$ ). Figure 4(a) shows  $\Delta R_L(\zeta, z)$  at the pulse center  $\zeta = 0$  (solid curve) and the front of the pulse  $\zeta = L$  (dashed curve), whereas Fig. 4(b) shows  $\Delta R_L(z)$  at the pulse center  $\zeta = 0$  (solid curve) and the back of the pulse  $\zeta = -L$  (dotted curve). Note that  $\Delta R_L(z)$  obtains a maximum of  $\Delta R_L = \exp(\zeta^2/L^2)$  at  $z/Z_\beta = -\zeta/L$ , e.g., a maximum of  $\Delta R_L = 2.82$  at  $z = Z_\beta$  for  $\zeta = -L$ . The physical interpretation of Eqs. (27) and (30)–(32) for the local betatron radius becomes ambiguous when  $\zeta^2 \gg L^2$ , since the pulse intensity becomes vanishingly small in these regions.

It is also insightful to define the *global* intensity-weighted mean-squared radius for the entire pulse via

$$\langle\langle r^2 \rangle\rangle = \frac{\int_{-\infty}^{\infty} d\zeta \int_0^\infty dr r^3 |\hat{a}|^2}{\int_{-\infty}^{\infty} d\zeta \int_0^\infty dr r |\hat{a}|^2}. \quad (34)$$

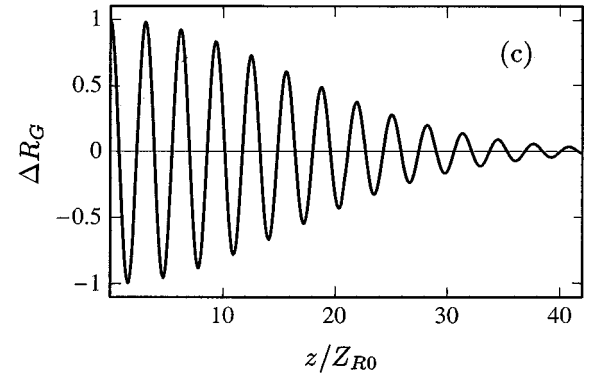
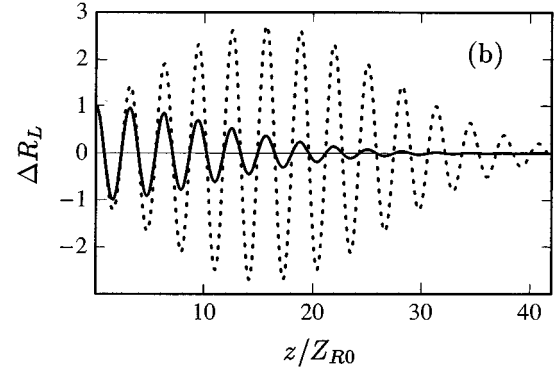
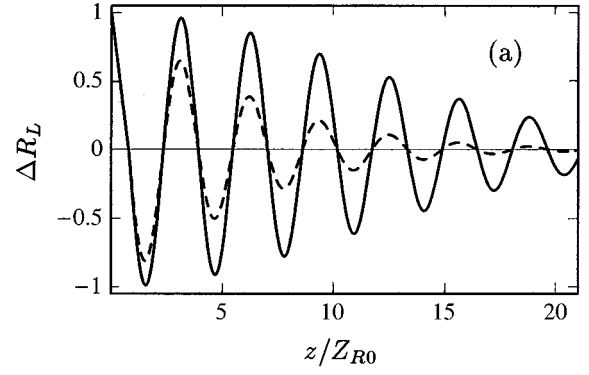


FIG. 4. Normalized local  $\Delta R_L(\zeta, z)$ , Eq. (32), and global  $\Delta R_G(z)$ , Eq. (37), RMS radius of the betatron oscillation vs  $z/Z_{R0}$  for  $Z_\beta = 5\pi Z_{R0}$ . (a) shows  $\Delta R_L$  at the center  $\zeta = 0$  (solid curve) and the front  $\zeta = L$  (dashed curve) of the pulse; (b) shows  $\Delta R_L$  at the center  $\zeta = 0$  (solid curve) and the back  $\zeta = -L$  (dotted curve) of the pulse; and (c) shows  $\Delta R_G$ .

This quantity is of relevance to a diagnostic that measures the time-integrated pulse intensity profile. For a Gaussian axial profile,

$$\int_{-\infty}^{\infty} d\zeta \int_0^\infty dr r |\hat{a}|^2 = \left(\frac{\pi}{2}\right)^{1/2} L \frac{r_0^2}{4} a_0^2, \quad (35)$$

which indicates that the total pulse energy is constant, and

$$\langle\langle r^2 \rangle\rangle = \frac{r_0^2}{2} \left[ 1 + 2 \frac{\delta r_0}{r_0} \Delta R_G(z) \right], \quad (36)$$

where

$$\Delta R_G = \exp\left(-\frac{z^2}{2Z_\beta^2}\right) \cos(k_{\beta 0} z) \quad (37)$$

is the normalized global intensity-weighted RMS betatron radius. Hence, for the entire pulse, the betatron oscillation damps via  $\exp(-z^2/2Z_\beta^2)$ . The normalized global RMS radius of the betatron oscillation  $\Delta R_G(z)$ , Eq. (37), is plotted in Figs. 4(c) versus  $z/Z_{R0}$  for the parameters  $\lambda_0 = 1 \mu\text{m}$ ,  $L = 5 \mu\text{m}$ , and  $r_0 = 10 \mu\text{m}$  ( $Z_\beta = 5\pi Z_{R0}$  and  $Z_{R0} = 310 \mu\text{m}$ ).

### B. Second-order dispersion

For the case of an axial Gaussian profile,  $b_0(\zeta) = a_0 \exp(-z^2/L^2)$ , the inverse Fourier transform to Eq. (23) can be obtained while retaining terms in the exponent to order  $\delta k^2/k_0^2$ . Specifically, the approximations  $k_\beta \approx k_{\beta 0}(1 - \delta k/k_0 + \delta k^2/k_0^2)$  and  $\delta k^2 z/k \approx \delta k^2 z/k_0$  are made in the exponent of Eq. (23). This indicates  $\hat{a} = \hat{a}_0 + \delta \hat{a}$ , where  $\hat{a}_0$  is the matched pulse solution given by Eq. (18) and

$$\begin{aligned} \delta \hat{a} = & -a_0 \frac{\delta r_0}{r_0} \left(1 - \frac{2r^2}{r_0^2}\right) (1 + \eta_1^2)^{-1/4} \\ & \times \exp\left[-\frac{r^2}{r_0^2} - \frac{\zeta_1^2}{L^2} \frac{(1-i\eta_1)}{(1+\eta_1^2)} - \frac{i}{2} \tan^{-1} \eta_1 - ik_{\beta 0} z\right], \end{aligned} \quad (38)$$

where  $\zeta_1 = \zeta + k_{\beta 0} z/k_0$ ,  $\eta_1 = z/Z_{D1}$ , and

$$Z_{D1} = \frac{k_0 L^2/2}{(1 - \beta_{g0}^2 + 2k_{\beta 0}/k_0)} \approx \frac{(\pi L/\lambda_0)^2 Z_{R0}}{(3 + k_{\beta 0}^2 r_0^2/4)} \quad (39)$$

is the dispersion length for the perturbed field. Equation (38) can be interpreted as a matched first-order ( $m=1, p=0$ ) Laguerre-Gaussian mode, including the effects of second-

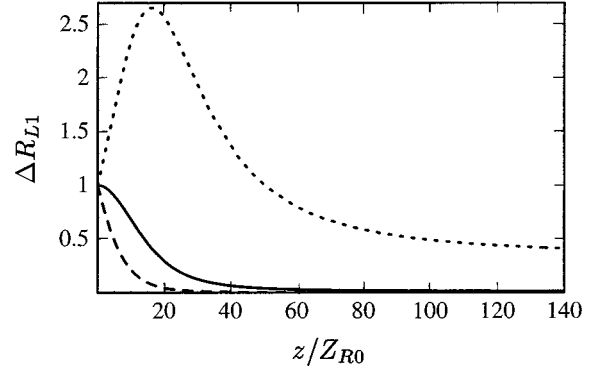


FIG. 5. Normalized local RMS betatron amplitude  $\Delta R_{L1}(\zeta, z)$ , Eq. (44), vs  $z/Z_{R0}$  at the center  $\zeta=0$  (solid curve), the front  $\zeta = L_{e0}(z)$  (dashed curve), and the back  $\zeta = -L_{e0}(z)$  (dotted curve) of the pulse, for  $Z_\beta = 5\pi Z_{R0}$ ,  $Z_{D0} = 46Z_{R0}$ , and  $Z_{D1} = 33Z_{R0}$ .

order dispersion (see Appendix C). Notice that the dispersion length for the perturbation  $Z_{D1}$  is shorter than that for the matched solution  $Z_{D0}$ , i.e.,

$$Z_{D1}^{-1} - Z_{D0}^{-1} = 4k_{\beta 0}/k_0^2 L^2 = 2Z_{R0}/Z_\beta^2. \quad (40)$$

This is a result of the reduced group velocity of the perturbation,  $\beta_{g1} < \beta_{g0}$ , since, as before,  $\delta \hat{a}$  is a first-order Laguerre-Gaussian mode. In particular, Eq. (39) can be written as  $Z_{D1} \approx (k_0 L^2/2)(1 - \beta_{g1}^2)^{-1}$ , where  $\beta_{g1}$  is given by Eq. (26). The effective axial pulse length associated with the perturbed field, Eq. (38), is

$$L_{e1} = L(1 + z^2/Z_{D1}^2)^{1/2}. \quad (41)$$

The intensity profile, to first order in  $\delta r_0/r_0$ , is given by  $|\hat{a}|^2 = \hat{I}_0 + \delta \hat{I}$ , where  $\hat{I}_0 = |\hat{a}_0|^2$  is the matched pulse solution given by Eq. (21), and  $\delta \hat{I} = \hat{a}_0 \delta \hat{a}^* + \hat{a}_0^* \delta \hat{a}$ , i.e.,

$$\delta \hat{I} \approx -\frac{2a_0^2 L}{L_{e0}^{1/2} L_{e1}^{1/2}} \frac{\delta r_0}{r_0} \left(1 - \frac{2r^2}{r_0^2}\right) \exp\left[-\frac{2r^2}{r_0^2} - \frac{\zeta^2}{L_{e0}^2} - \frac{\zeta_1^2}{L_{e1}^2}\right] \cos\left[k_{\beta 0} z + \frac{\eta_0 \zeta^2}{L_{e0}^2} - \frac{\eta_1 \zeta_1^2}{L_{e1}^2} - \frac{1}{2} \tan^{-1} \eta_0 + \frac{1}{2} \tan^{-1} \eta_1\right], \quad (42)$$

where  $\eta_0 = z/Z_{D0}$  and  $\eta_1 = z/Z_{D1}$ .

The local intensity-weighted mean-squared radius, as defined by Eq. (27), is given by

$$\langle r^2 \rangle \approx \frac{r_0^2}{2} \left\{ 1 + 2 \frac{\delta r_0}{r_0} \Delta R_{L1}(\zeta, z) \cos\left[k_{\beta 0} z + \frac{\eta_0 \zeta^2}{L_{e0}^2} - \frac{\eta_1 \zeta_1^2}{L_{e1}^2} - \frac{1}{2} \tan^{-1} \eta_0 + \frac{1}{2} \tan^{-1} \eta_1\right] \right\}, \quad (43)$$

where

$$\Delta R_{L1} = \left(\frac{L_{e0}}{L_{e1}}\right)^{1/2} \exp\left[\frac{\zeta^2}{L_{e0}^2} - \frac{L^2}{L_{e1}^2} \left(\frac{\zeta}{L} + \frac{z}{Z_\beta}\right)^2\right] \quad (44)$$

is the normalized amplitude of the local RMS radius of the betatron oscillation, and  $L_{e0}(z)$  and  $L_{e1}(z)$  are given by Eqs.

(20) and (41), respectively. At the pulse center  $\zeta=0$ , the betatron oscillation damps via  $\exp(-z^2/Z_{\beta 1}^2)$ , where

$$Z_{\beta 1} = (k_0 L_{e1}/2) Z_{R0}. \quad (45)$$

Notice that the damping distance is increased due to dispersion,  $Z_{\beta 1} = Z_{\beta 0}(1 + z^2/Z_{D1}^2)^{1/2}$ . The normalized local RMS betatron amplitude  $\Delta R_{L1}(\zeta, z)$ , Eq. (44), is plotted in Fig. 5 versus  $z/Z_{R0}$  at the pulse center  $\zeta=0$  (solid curve), as well

as at the front  $\zeta=L_{e0}(z)$  (dashed curve), and the back  $\zeta=-L_{e0}(z)$  (dotted curve) of the pulse, for the parameters  $\lambda_0=1\ \mu\text{m}$ ,  $L=5\ \mu\text{m}$ ,  $r_0=10\ \mu\text{m}$ , and  $\lambda_p=15\ \mu\text{m}$  ( $Z_\beta=16Z_{R0}$ ,  $Z_{D0}=46Z_{R0}$ , and  $Z_{D1}=33Z_{R0}$ ). Again, there is a head-tail asymmetry. This asymmetry is complicated by the fact that the matched solution and the perturbed solution are characterized by different dispersion lengths,  $Z_{D0}>Z_{D1}$ . Asymptotically, for  $z^2\gg Z_{D0}^2$ , the local RMS amplitude  $\Delta R_{L1}(z)$  damps to a finite value. Specifically, at the pulse center  $\zeta=0$ ,

$$\Delta R_{L1}(0)\rightarrow\left(\frac{Z_{D1}}{Z_{D0}}\right)^{1/2}\exp\left(-\frac{Z_{D1}^2}{Z_\beta^2}\right), \quad (46)$$

whereas at the front and back of the pulse  $\zeta=\pm L_{e0}(z)$ ,

$$\Delta R_{L1}(\pm L_{e0})\rightarrow\left(\frac{Z_{D1}}{Z_{D0}}\right)^{1/2}\exp\left[1-\left(\frac{Z_{D1}\pm Z_{D1}}{Z_\beta}\pm\frac{Z_{D1}}{Z_{D0}}\right)^2\right]. \quad (47)$$

For the parameters of Fig. 5,  $\Delta R_{L1}(0)\rightarrow 9.3\times 10^{-3}$ ,  $\Delta R_{L1}(L_{e0})\rightarrow 6.7\times 10^{-4}$ , and  $\Delta R_{L1}(-L_{e0})\rightarrow 0.33$ . As before, the physical interpretation of  $\langle r^2 \rangle$  becomes ambiguous in the region  $\zeta^2\gg L_{e0}^2$ , since the intensity in that region is vanishingly small.

The *global* intensity-weighted mean-squared radius, as defined by Eq. (34), including the effects of second-order dispersion is given by

$$\begin{aligned} \langle\langle r^2 \rangle\rangle &\approx \frac{r_0^2}{2} \left\{ 1 + 2 \frac{\delta r_0}{r_0} \Delta R_{G1}(z) \right. \\ &\quad \left. \times \cos \left[ k_{\beta 0} z \frac{(1+3z^2 Z_{R0}^2/2Z_\beta^4)}{(1+z^2 Z_{R0}^2/Z_\beta^4)} + \frac{1}{2} \tan^{-1} \left( \frac{z Z_{R0}}{Z_\beta} \right) \right] \right\}, \end{aligned} \quad (48)$$

where

$$\Delta R_{G1} = \left( 1 + \frac{z^2 Z_{R0}^2}{Z_\beta^4} \right)^{-1/4} \exp \left[ -\frac{z^2/2Z_\beta^2}{(1+z^2 Z_{R0}^2/Z_\beta^4)} \right] \quad (49)$$

is the normalized amplitude of the global RMS betatron oscillation and the relation  $\eta_1 - \eta_0 = 2z Z_{R0}/Z_\beta^2$  has been used. The normalized global RMS betatron amplitude  $\Delta R_{G1}(z)$  is plotted in Fig. 6 for the parameters  $Z_\beta=5\pi Z_{R0}$  (solid curve),  $Z_\beta=10Z_{R0}$  (dashed curve), and  $Z_\beta=30Z_{R0}$  (dotted curve).

## V. NONLINEAR EFFECTS

The above theory assumed  $a^2\ll 1$  and  $P/P_c\ll 1$ , i.e., nonlinear effects were neglected. At high intensity and/or power, nonlinear effects could play an important role in pulse propagation in channels. For example, intense laser pulses are subject to various instabilities. Two important instabilities are the self-modulation and the laser-hose instability [2,33,42–46]. In the short pulse regime, these instabilities will undergo exponential growth  $\exp(N_e)$  with the number of *e*-foldings given by [2,46]

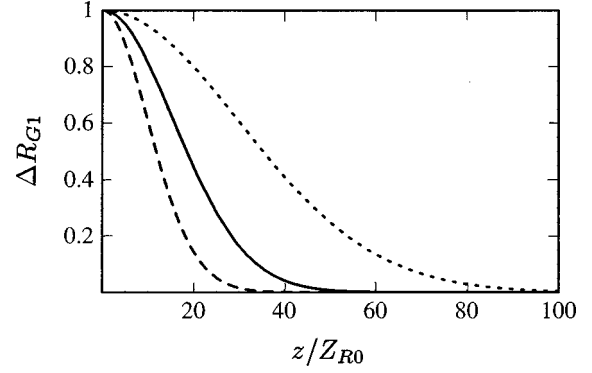


FIG. 6. Normalized global RMS betatron amplitude  $\Delta R_{G1}(z)$ , Eq. (49), vs  $z/Z_{R0}$  for the parameters  $Z_\beta=5\pi Z_{R0}$  (solid curve),  $Z_\beta=10Z_{R0}$  (dashed curve), and  $Z_\beta=30Z_{R0}$  (dotted curve).

$$N_e \approx 1.3 \left( \frac{P}{P_c} k_p^2 \xi^2 \frac{z}{Z_R} \right)^{1/3}, \quad (50)$$

where  $P/P_c \approx k_p^2 r_0^2 a_0^2/32$ . Note that the number of *e*-foldings scales with power *P*, density  $n_0$ , and pulse length *L* as  $N_e \sim (P n_0^2 L^2)^{1/3}$ . In terms of the betatron damping length  $Z_\beta$ , the number of *e*-foldings at the end of the pulse  $|\zeta|=L$  is given by

$$N_e \approx 6.5 \left( \frac{P}{P_c} \frac{L^3}{\lambda \lambda_p^2} \frac{z}{Z_\beta} \right)^{1/3}. \quad (51)$$

It is insightful to estimate how much growth of the hose-modulation instability one might expect after propagating a distance equal to a betatron damping distance  $z \approx Z_\beta$ . For a plasma density of  $n_0=10^{17}\ \text{cm}^{-3}$  and a laser pulse with  $\lambda=1\ \mu\text{m}$  and  $L=5\ \mu\text{m}$  (a full width at half maximum intensity duration of 20 fs), the number of *e*-foldings is  $N_e \approx 0.25$  for  $P=1\ \text{TW}$  and  $N_e \approx 0.54$  for  $P=10\ \text{TW}$ . Hence, no appreciable growth of the instability is expected at this density. As another example, the density range for which the laser-hose instability will be amplified by less than a factor of 100 can be estimated. Requiring  $N_e < 4.6$  after  $z=Z_\beta$  implies  $n_0 < 7.9 \times 10^{18}\ \text{cm}^{-3}$  for  $P=1\ \text{TW}$  and  $n_0 < 2.5 \times 10^{18}\ \text{cm}^{-3}$  for  $P=10\ \text{TW}$ .

It is also important to note that the growth rate Eq. (50) for the hose-modulation instability was obtained from a paraxial theory, i.e., the cross derivative term  $\partial^2/\partial \xi \partial z$  in the wave equation for the slowly varying amplitude Eq. (8) has been neglected. The effects of the dispersive term  $\partial^2/\partial \xi \partial z$  become very important for ultrashort pulses. This paper has addressed the effects of this term in the limits of low power and low intensity. Theories of laser-plasma instabilities that are valid for finite profile, ultrashort pulses that include the effects of the dispersive term are currently lacking in the literature. Based on the results obtained in this paper, however, some dispersive effects on instabilities of ultrashort pulses can be estimated. When a matched, fundamental Gaussian pulse (characterized by the mode numbers  $m=0$  and  $p=0$  as discussed in Appendix C) goes unstable in a plasma channel, it will generate higher-order modes, e.g., the  $m \geq 1, p=0$  mode in the case of self-modulation or the *m*



$=0, p \geq 1$  mode in the case of the laser hose. As noted in Appendix C, these modes propagate at different group velocities,

$$\beta_g \approx 1 - k_p^2/2k_0^2 - 2(2m+p+1)/k_0^2 r_0^2. \quad (52)$$

Hence, the excited modes will propagate out of the region of the fundamental pulse when the group velocity slippage distance becomes comparable to the pump pulse length, i.e.,  $z\Delta\beta_g \approx L$ , where  $\Delta\beta_g = \beta_{g0} - \beta_g$  and  $\beta_{g0} = \beta_g(m=0, p=0)$ . This occurs after a propagation distance

$$z \approx k_0 L Z_{R0} / (2m+p), \quad (53)$$

i.e.,  $z \sim Z_\beta$  for  $m \sim 1$  or  $p \sim 1$ . Hence, the growth of the hose-modulation instability will become significantly altered and/or suppressed after a distance on the order of the betatron damping distance,  $z \approx Z_\beta$ .

## VI. DISCUSSION

The propagation characteristics of an ultrashort laser pulse in a preformed plasma channel have been analyzed. The plasma channel is assumed to be parabolic with a density profile of the form  $n(r) = n_0 + \Delta n r^2 / r_0^2$ . The laser pulse was assumed to have  $P/P_c \ll 1$  and  $a_0^2 \ll 1$ , such that nonlinear effects (e.g., relativistic self-focusing) could be neglected and the channel could be assumed unperturbed by the laser pulse. Solutions to the wave equation beyond the paraxial approximation were derived that include finite pulse length effects and group velocity dispersion. The laser field is given by  $a_x = \hat{a} \exp(ik_0 z - i\omega_0 t) + \text{c.c.}$ , where the field envelope  $\hat{a}(r, z, \zeta)$  evolves via Eq. (8). The field envelope is obtained by performing a single integral over  $\delta k$ ,  $\hat{a} = (2\pi)^{-1/2} \int_{-\infty}^{\infty} d\delta k \exp(i\delta k \zeta) \hat{a}_k$ , where  $\hat{a}_k$  is given by Eq. (11) along with the definitions in Eqs. (12a)–(12d). For completeness, the plasma source current is discussed in Appendix A, the evolution of ultrashort laser pulses in the absence of a density channel ( $\Delta n = 0$ ) is discussed in Appendix B, and a generalization of the results to include high-order modes is discussed in Appendix C.

Since the condition for guiding a particular  $k = k_0 + \delta k$  mode with a constant spot size  $r_s = r_0$  is given by  $\Delta n = \Delta n_c = 1/\pi r_e r_0^2$  and is independent of  $k$ , matched beam solutions exist wherein the entire pulse can propagate with a nonevolving radial profile, i.e., a normalized intensity profile  $|\hat{a}|^2 \sim a_0^2 \exp(-2r^2/r_0^2)$ . Group velocity dispersion effects were included in the matched beam solution to second order in the parameter  $\delta k/k_0$ . This results in spreading of the pulse length, i.e.,  $|\hat{a}|^2 \sim a_0^2 (L/L_{e0}) \exp(-2\zeta^2/L_{e0}^2)$ , where  $L$  is the initial pulse length,  $L_{e0} = L(1 + z^2/Z_{D0}^2)^{1/2}$ , and  $Z_{D0} = \gamma_{g0}^2 k_0 L^2 / 2$  is the dispersion length for a matched pulse. Here,  $\gamma_{g0}^2 = (1 - \beta_{g0}^2)^{-1}$  and  $v_{g0} = c\beta_{g0}$  is the group velocity of a matched pulse in a channel, i.e.,  $\gamma_{g0}^2 = (\omega_0/\omega_p)^2 (1 + 4/k_p^2 r_0^2)^{-1}$ . In terms of the group velocity dispersion parameter  $\beta_2$  often quoted in fiber optics [47],  $Z_{D0} = L^2/2|\beta_2|c^2$ , where  $\beta_2 = -v_g^{-2} dv_g/d\omega$  and  $v_g$  is the group velocity. For a plasma  $\beta_2 \approx -(1 - \beta_{g0}^2)/\omega_0 c$ . Since  $\beta_2 < 0$ , the dispersion is anomalous.

A pulse which is not properly matched into a channel undergoes betatron oscillations in its envelope. For example,

if at the channel entrance  $r_s(z=0) = r_0 + \delta r_0$  and  $dr_s/dz = 0$  with  $\delta r_0/r_0 \ll 1$ , then the spot size associated with a given  $k = k_0 + \delta k$  mode undergoes betatron oscillations about the matched spot size  $r_0$  of the form  $r_s = r_0 + \delta r_0 \cos k_\beta z$ , where  $k_\beta = 2/Z_R$  is the betatron wave number and  $Z_R = kr_0^2/2$ . A finite pulse length  $L$  leads to a spread in laser wave numbers  $|\delta k| \sim 1/L$  and, hence, a spread in betatron wave numbers. This results in phase mixing and damping of the betatron oscillations. In particular, for a slight mismatch  $\delta r_0^2/r_0^2 \ll 1$ , the RMS radius of the pulse exhibits betatron oscillations of the form given by Eqs. (30)–(32) and (36)–(37). The global RMS betatron amplitude damps via  $\exp(-z^2/2Z_\beta^2)$ , where  $Z_\beta = (k_0 L/2)Z_{R0} = (k_0 r_0/2)^2 L$  is the betatron damping distance.

An alternative interpretation for the laser envelope betatron oscillations and their subsequent damping is the following. To lowest order in  $\delta r_0/r_0$ , a mismatched laser pulse in a channel is a superposition of two matched modes: a fundamental Gaussian mode,  $\hat{a}_0$ , and a first-order, axisymmetric Laguerre-Gaussian mode,  $\delta \hat{a}$ , the amplitude of which is proportional to  $\delta r_0/r_0$ . The relative axial wave-number shift between the fundamental and higher-order mode is given by  $\Delta k_z \approx -2(2m+p)/k_0 r_0^2 = -k_\beta$  for  $m=1$  and  $p=0$ , i.e., a relative phase shift of  $\Delta\theta = -k_\beta z$ . Hence, the first-order correction to the field envelope oscillates relative to the fundamental at the betatron wave number, i.e., via  $\cos(k_\beta z)$ . Furthermore, the axial group velocity of the first-order mode  $\beta_{g1} \approx c(k_0 + \Delta k_z)/\omega_0$  is less than that of the fundamental  $\beta_{g0} = ck_0/\omega_0$  by an amount  $\beta_{g0} - \beta_{g1} \approx -\Delta k_z/k_0 \approx k_\beta/k_0$ .

The amplitude of the betatron oscillation, as defined by the intensity-weighted RMS radius of the pulse, is determined by the interference between the two modes, i.e., dependent on the product  $\hat{a}_0 \delta \hat{a}$ . As the first-order mode slips behind the fundamental, the relative contribution of the first-order mode to the spot size decreases at the front ( $\zeta > 0$ ) and increases at the back ( $\zeta < 0$ ) of the pulse. This results in an asymmetry in the betatron oscillation, i.e., the apparent amplitude initially decreases at the front and increases at the back of the pulse. As the slippage continues, the two modes overlap less and less, resulting in an overall decrease in the betatron amplitude, i.e., damping. The characteristic damping distance is determined by when the slippage distance  $\Delta L_s = (\beta_{g0} - \beta_{g1})z$  becomes comparable to the pulse length, i.e.,  $\Delta L_s \approx L$ , which gives  $z \approx k_0 L/k_\beta = Z_\beta$ . In terms of the axial pulse profile  $b_0(\zeta)$ , the local RMS betatron amplitude is proportional to  $b_0(\zeta_1)/b_0(\zeta)$ , where  $\zeta = z - \beta_{g0} ct$  and  $\zeta_1 = z - \beta_{g1} ct$ . For Gaussian axial profiles, this gives the damping behavior indicated by Eqs. (30)–(32).

The effects of second-order group velocity dispersion were also included in the analysis of mismatched propagation in a channel. It was found that the perturbed component of the radiation field, proportional to  $\delta r_0/r_0$ , undergoes enhanced dispersive spreading that is characterized by the dispersion length  $Z_{D1} = \gamma_{g1}^2 k_0 L^2 / 2$ , where  $\gamma_{g1}^2 \approx (\omega_0/\omega_{p0})^2 (1 + 12/k_p^2 r_0^2)^{-1}$ . The decrease in the dispersion length is due to a decrease in the group velocity associated with the first-order mode of the perturbed field, i.e.,  $\gamma_{g1}^2 = (1 - \beta_{g1}^2)^{-1}$ .

Experimentally, for a long channel  $z > Z_\beta$ , the high-order

modes representing the envelope mismatch should be observed to emerge behind the fundamental Gaussian pulse. The first-order mode will become “well-separated” from the fundamental when the slippage length exceeds the sum of the dispersively broadened pulse lengths, i.e.,  $\Delta L_s > L_{e0} + L_{e1}$ , which gives  $z/Z_\beta > (L_{e0} + L_{e1})/L$ , where  $L_{e0,1} = L(1 + z/Z_{D0,1})^{1/2}$  and  $Z_{D0,1}$  are the dispersion lengths. Since typically  $Z_\beta < Z_{D1} < Z_{D0}$ , the modes should become well-separated for  $z > 2Z_\beta$ . To correctly determine the temporal intensity profile emerging from a long channel, corrections of order  $\delta r_0^2/r_0^2$  (or higher) need to be retained in the determination of the perturbed field  $\delta\hat{a}$ , which can be accomplished by retaining higher-order terms in the expansion of Eqs. (11)–(16). In addition, experimentally realizable channel profiles can be “leaky” and less apt to guide high-order modes [13,14,48]. This leakage of the higher-order modes constituting the envelope mismatch can lead to an enhanced damping of the betatron oscillation.

The damping of betatron oscillations in the pulse envelope and the dispersive spreading of the pulse length are important for short pulses propagating in long channels. Consider a  $\lambda_0 = 1 \mu\text{m}$  laser with a matched spot radius of  $r_0 = 10 \mu\text{m}$  and a Gaussian axial profile with  $L = 5 \mu\text{m}$ , which corresponds to a full width at half maximum of the intensity profile of  $L_{\text{FWHM}} = (2 \ln 2)^{1/2} L = 5.9 \mu\text{m}$  (20 fs). The plasma channel is parabolic,  $n = n_0 + \Delta n r^2/r_0^2$ , with  $\Delta n = \Delta n_c = 1.1 \times 10^{18} \text{ cm}^{-3}$  and  $n_0 = 4.9 \times 10^{18} \text{ cm}^{-3}$  ( $\lambda_p = 15 \mu\text{m}$ ). The matched Rayleigh length is  $Z_{R0} = \pi r_0^2/\lambda_0 = 310 \mu\text{m}$  and the betatron wavelength is  $\lambda_\beta = 2\pi/k_\beta = \pi Z_{R0} = 990 \mu\text{m}$ . The betatron damping length is  $Z_{\beta 0} \approx (\pi L_0/\lambda_0) Z_{R0} = 5\pi Z_{R0} = 0.49 \text{ cm}$ , e.g., after  $z = 1 \text{ cm}$  ( $32Z_{R0}$ ) the global betatron amplitude would be damped by a factor  $\exp(-z^2/2Z_{\beta 0}^2) = 0.12$ . Hence, for a long channel,  $z^2 \gg Z_{\beta 0}^2$ , a mismatched pulse would emerge at essentially the matched radius  $r_0$ . For these parameters, the dispersion length for a matched laser pulse  $Z_{D0} \approx (\pi^2 L^2/\lambda_0^2) \times (1 + \pi^2 r_0^2/\lambda_p^2)^{-1} Z_{R0}$  is  $Z_{D0} = 46Z_{R0} = 1.4 \text{ cm}$ . Hence, after propagating a distance of  $z = 100Z_{R0} = 3.1 \text{ cm}$ , the pulse length would spread to a length  $L_{e0} = 2.4L = 12 \mu\text{m}$  (a duration of 47 fs).

### ACKNOWLEDGMENTS

This work was supported by the Department of Energy. The authors acknowledge useful conversations with R. F. Hubbard and H. M. Milchberg.

### APPENDIX A: PLASMA SOURCE TERM

This appendix concerns corrections that may arise in the plasma source term  $\mathbf{S}_\perp$  due to the effects of a finite normalized electrostatic potential  $\phi = e\Phi/m_e c^2$ . In Coulomb gauge,  $\nabla \cdot \mathbf{a} = \mathbf{0}$ , the normalized transverse wave equation is given by

$$\left( \nabla^2 - \frac{\partial^2}{\partial ct^2} \right) \mathbf{a}_\perp = \mathbf{S}_\perp, \quad (\text{A1})$$

$$\mathbf{S}_\perp = k_p^2 \frac{n}{n_0} \boldsymbol{\beta}_\perp + \frac{\partial}{\partial ct} \nabla_\perp \phi, \quad (\text{A2})$$

where  $n$  is the plasma density,  $n_0$  is the ambient density along the channel axis,  $k_p^2 = 4\pi n_0 e^2/m_e c^2$ ,  $\boldsymbol{\beta} = \mathbf{v}/c$  is the normalized plasma fluid velocity, and  $(n/n_0)\boldsymbol{\beta}_\perp$  is the normalized transverse plasma current in the fluid approximation. Here,  $n$  and  $\boldsymbol{\beta}$  are assumed to obey the relativistic cold fluid equations

$$(\partial/\partial ct + \boldsymbol{\beta} \cdot \nabla) \mathbf{u} = \partial \mathbf{a} / \partial ct + \nabla \phi - \boldsymbol{\beta} \times (\nabla \times \mathbf{a}), \quad (\text{A3})$$

$$\partial n / \partial ct + \nabla \cdot (n \boldsymbol{\beta}) = 0, \quad (\text{A4})$$

$$\nabla^2 \phi = k_p^2 (n - n_e) / n_0, \quad (\text{A5})$$

where  $\mathbf{u} = \gamma \boldsymbol{\beta}$ ,  $\gamma = (1 - \beta^2)^{-1/2}$ , and  $n_e(r)$  is the equilibrium plasma density, which is assumed to be a parabolic channel of the form  $n_e = n_0 + \Delta n r^2/r_0^2$ .

Assuming  $a^2 \ll 1$ , the perturbed fluid quantities  $\delta n$ ,  $\delta \boldsymbol{\beta}$ , and  $\delta \phi$ , to first order in  $|a|$ , obey the equations

$$\partial \delta \boldsymbol{\beta} / \partial ct = \partial \mathbf{a} / \partial ct + \nabla \delta \phi, \quad (\text{A6})$$

$$\partial \delta n / \partial ct + \nabla \cdot (n_e \delta \boldsymbol{\beta}) = 0, \quad (\text{A7})$$

$$\nabla^2 \delta \phi = k_p^2 \delta n / n_0. \quad (\text{A8})$$

Combining Eqs. (A6)–(A8) yields

$$(\partial^2 / \partial ct^2 + k_p^2) \nabla^2 \delta \phi + (\partial \mathbf{a} / \partial ct + \nabla \delta \phi) \cdot \nabla k_p^2 = 0, \quad (\text{A9})$$

where  $k_p^2 = k_p^2 n_e(r) / n_0 = k_p^2 (1 + \Delta n r^2 / n_0 r_0^2)$ . Assuming  $a \sim \exp(ik_0 z - i\omega_0 t)$  and  $\delta \phi \sim \exp(ik_0 z - i\omega_0 t)$ , it is straightforward to find the leading-order contribution to  $\delta \boldsymbol{\beta}_\perp$  and  $\delta \phi$ , i.e.,

$$\delta \boldsymbol{\beta}_\perp \approx \mathbf{a}_\perp + i \nabla_\perp \delta \phi / k_0, \quad (\text{A10})$$

$$\delta \phi \approx i (\mathbf{a}_\perp \cdot \nabla_\perp k_p^2) / k_0^3. \quad (\text{A11})$$

Similarly, the leading-order correction to the source term, Eq. (A2), is given by

$$\begin{aligned} \mathbf{S}_\perp &\approx k_p^2 \mathbf{a}_\perp - ik_0 (1 - k_p^2/k_0^2) \nabla_\perp \delta \phi \\ &\approx k_p^2 \mathbf{a}_\perp + \nabla_\perp (\mathbf{a}_\perp \cdot \nabla_\perp k_p^2) / k_0^2. \end{aligned} \quad (\text{A12})$$

For a parabolic density channel,  $\nabla_\perp k_p^2 \sim k_p^2 \Delta n_c / n_0 r_0 \sim 4/r_0^3$ , where  $\Delta n_c = 1/\pi r_e r_0^2$  is the critical channel depth. Hence, the correction to the source term  $\delta \mathbf{S}_\perp = \mathbf{S}_\perp - k_p^2 \mathbf{a}_\perp$  scales as

$$\delta \mathbf{S}_\perp \approx \nabla_\perp (\mathbf{a}_\perp \cdot \nabla_\perp k_p^2) / k_0^2 \sim 4 \mathbf{a}_\perp / k_0^2 r_0^4 \sim \mathbf{a}_\perp / Z_{R0}^2, \quad (\text{A13})$$

where  $Z_{R0} = k_0 r_0^2 / 2$  is the Rayleigh length.

The correction to the source term  $\delta \mathbf{S}_\perp$  can be neglected provided that it is small in comparison to the terms retained in the wave equation for the pulse envelope  $\hat{a}$ , Eq. (8), which is written in terms of the independent variables  $\zeta = z - \beta_{g0} ct$  and  $z$ . Since the term  $\partial^2 \hat{a} / \partial z^2 \sim \hat{a} / Z_{R0}^2$  was neglected in Eq. (8), so can the term  $\delta \mathbf{S}_\perp \sim \hat{a} / Z_{R0}^2$  be neglected. The conditions for validity of neglecting this term are discussed in the paragraph following Eq. (8). Specifically, this

requires (i)  $|\partial^2 \hat{a}/\partial z^2| \ll 2|\partial^2 \hat{a}/\partial \zeta \partial z|$ , which implies  $L \ll 2Z_{R0}$ , and (ii)  $|\partial^2 \hat{a}/\partial z^2| \ll (1 - \beta_{g0}^2)|\partial^2 \hat{a}/\partial \zeta^2|$ , which implies  $L^2/r_0^2 \ll (1 + k_{p0}^2 r_0^2/4)$ .

## APPENDIX B: DIFFRACTING PULSES

In this appendix, the evolution of short laser pulses in uniform plasmas is analyzed. In the absence of a channel, the evolution of the Fourier transform of the pulse envelope  $\hat{a}_k$  is described by Eq. (9) with  $\Delta n = 0$ , i.e.,

$$\left( \nabla_{\perp}^2 + 2ik \frac{\partial}{\partial z} \right) \hat{a}_k = [k_{p0}^2 - k_0^2(\beta_{p0}^2 - 1) + \delta k^2(1 - \beta_{g0}^2)] \hat{a}_k, \quad (\text{B1})$$

where  $k = k_0 + \delta k$  and the  $\partial^2/\partial z^2$  term has been neglected in the wave operator. The total transverse laser field is  $a_x = \hat{a} \exp(ik_0 z - i\omega_0 t) + \text{c.c.}$ , where the laser field envelope is given by

$$\hat{a}(r, z, \zeta) = \frac{1}{\sqrt{2\pi}} \int_{-\infty}^{\infty} d\delta k \exp(i\delta k \zeta) \hat{a}_k(r, z, k). \quad (\text{B2})$$

Here,  $\zeta = z - \beta_{g0} ct$ , where  $\beta_{g0}^2 = \beta_{p0}^{-2} = 1 - \omega_{p0}^2/\omega_0^2 - 4c^2/\omega_0^2 r_0^2$ , with the pulse central frequency and wave number satisfying  $\omega_0^2/c^2 - k_0^2 = k_{p0}^2 + 4/r_0^2$ . As is shown below,  $v_{g0} = c\beta_{g0}$  is the group velocity of the pulse centroid at the focal point ( $z=0$ ).

Since Eq. (B1) has the form of a paraxial wave equation, solutions for  $\hat{a}_k$  can readily be found, e.g., the lowest-order Gaussian mode is given by

$$\hat{a}_k = b_k \exp[i\theta - (1 - i\alpha)r^2/r_s^2], \quad (\text{B3})$$

where the quantities  $b_k(k, z)$ ,  $\theta(k, z)$ ,  $\alpha(k, z)$ , and  $r_s(k, z)$ , which represent the amplitude, phase shift, curvature, and spot size of the field in  $k$  space, respectively, satisfy Eqs. (12a)–(12d). In the absence of a channel,  $\Delta n = 0$ , Eqs. (12a)–(12d) can be solved to describe a diffracting field. In particular, for the initial ( $z=0$ ) conditions  $r_s = r_0$ ,  $dr_s/dz = 0$ ,  $\alpha = 0$ ,  $\theta = 0$ , and  $b_k = b_{k0}$ , the solutions to Eqs. (12a)–(12d) are

$$\alpha = z/Z_R, \quad (\text{B4})$$

$$b_k = b_{k0} r_s / r_0, \quad (\text{B5})$$

$$r_s = r_0(1 + \alpha^2)^{1/2}, \quad (\text{B6})$$

$$\theta = \alpha - \tan^{-1} \alpha - (\delta k^2 r_0^2/4)(1 - \beta_{g0}^2)\alpha, \quad (\text{B7})$$

where  $Z_R = kr_0^2/2$  is the Rayleigh length associated with the total wave number  $k = k_0 + \delta k$ ,  $r_0$  is the minimum spot size at the focal point (assumed to be at  $z=0$ ), and  $b_{k0}$  is the initial  $\delta k$  spectrum of the laser pulse at  $z=0$ . Note that for an initial Gaussian axial pulse profile of the form  $b_0 = a_0 \exp(-\zeta^2/L^2)$ ,  $b_{k0} = a_0(L/\sqrt{2})\exp(-\delta k^2 L^2/4)$ . Furthermore, note that in the limit of a long laser beam, Eqs. (B4)–(B7) reduce to the usual paraxial solutions when  $\delta k = 0$ .

It is convenient to write  $\hat{a}_k$  in the form

$$\hat{a}_k = b_{k0} \exp(\psi_k), \quad (\text{B8})$$

where

$$\psi_k = -\frac{1}{2} \ln(1 + \alpha^2) - \frac{r^2/r_0^2}{(1 + i\alpha)} + i(\alpha - \tan^{-1} \alpha) - i\delta k^2 r_0^2(1 - \beta_{g0}^2) \frac{\alpha}{4}. \quad (\text{B9})$$

Since  $|\delta k| \sim 1/L \ll k_0$ , the inverse Fourier transform to Eq. (B8) can be found by expanding  $\psi_k(k_0 + \delta k)$  about  $k_0$ , i.e.,

$$\psi_k \approx \psi + \psi' \delta k + \psi'' \delta k^2/2, \quad (\text{B10})$$

where  $\psi = \psi_k(\delta k = 0)$ ,  $\psi' = (d\psi_k/d\delta k)(\delta k = 0)$ , and  $\psi'' = (d^2\psi_k/d\delta k^2)(\delta k = 0)$ . Specifically,

$$\psi = -\frac{1}{2} \ln(1 + \alpha_0^2) - \frac{r^2/r_0^2}{(1 + i\alpha_0)} + i(\alpha_0 - \tan^{-1} \alpha_0), \quad (\text{B11})$$

$$\psi' = \frac{\alpha_0}{k_0} \left[ \frac{\alpha_0}{(1 + i\alpha_0)} - \frac{ir^2/r_0^2}{(1 + i\alpha_0)^2} \right], \quad (\text{B12})$$

$$\psi'' = -\frac{\alpha_0}{k_0^2} \left[ \frac{(3\alpha_0 + 2i\alpha_0^2)}{(1 + i\alpha_0)^2} - \frac{2ir^2/r_0^2}{(1 + i\alpha_0)^3} + \frac{i}{2} k_0^2 r_0^2 (1 - \beta_{g0}^2) \right], \quad (\text{B13})$$

where  $\alpha_0 = z/Z_{R0}$  and  $Z_{R0} = k_0 r_0^2/2$ . Solutions for  $\hat{a}(\zeta)$  can be found order by order in the parameter  $|\delta k|/k_0 \sim 1/k_0 L$ .

### 1. Zeroth-order solution

The zeroth-order (paraxial) solution is given by

$$\begin{aligned} \hat{a}_0 &= b_0(\zeta) \exp(\psi) \\ &= b_0(\zeta) \frac{r_0}{r_{s0}} \exp \left[ -(1 - i\alpha_0) \frac{r^2}{r_{s0}^2} + i(\alpha_0 - \tan^{-1} \alpha_0) \right], \end{aligned} \quad (\text{B14})$$

where  $r_{s0} = r_0(1 + \alpha_0^2)^{1/2} = r_0(1 + z^2/Z_{R0}^2)^{1/2}$  is the zeroth-order (paraxial) laser spot size. Furthermore, note that the effective axial wave number associated with the laser field is given by  $k_z = k_0 + \partial\psi_i/\partial z$ , where  $\psi_i = \text{Im}(\psi)$ , i.e.,

$$k_z \approx k_0 + \frac{1}{Z_{R0}} \left[ \frac{\alpha_0^2}{(1 + \alpha_0^2)} + \frac{(1 - \alpha_0)^2}{(1 + \alpha_0^2)^2} \frac{r^2}{r_0^2} \right]. \quad (\text{B15})$$

### 2. First-order solution

To first order,  $\hat{a}_k = b_{k0} \exp(\psi + \psi' \delta k)$ . The inverse transform of this yields

$$\hat{a} = b_0(\zeta - i\psi') \exp(\psi). \quad (\text{B16})$$

For a Gaussian axial profile,  $b_0(\zeta) = a_0 \exp(-\zeta^2/L^2)$ , the normalized laser pulse intensity profile associated with the first-order solution is

$$|\hat{a}|^2 \approx a_0^2 \frac{r_0^2}{r_{s0}^2} \exp \left[ -\frac{2r^2}{r_{s0}^2} - \frac{2}{L^2} (\zeta + \psi'_i)^2 \right], \quad (\text{B17})$$

plus corrections of order  $|2\psi_r'/L^2| \sim 1/k_0^2 L^2$  (second order in the parameter  $|\delta k|/k_0$ ). Here,  $\psi_r'$  and  $\psi_i'$  refer to the real and imaginary parts of  $\psi'$ , respectively, i.e.,

$$\psi_r' = \frac{\alpha_0^2}{k_0(1+\alpha_0^2)} \left[ 1 - \frac{2r^2}{r_{s0}^2} \right], \quad (\text{B18})$$

$$\psi_i' = -\frac{\alpha_0}{k_0(1+\alpha_0^2)} \left[ \alpha_0^2 + (1-\alpha_0^2) \frac{r^2}{r_{s0}^2} \right]. \quad (\text{B19})$$

The local  $\zeta_L$  and global  $\zeta_G$  axial pulse centroids are defined by

$$\zeta_L = \frac{\int_{-\infty}^{\infty} d\xi \xi |\hat{a}|^2}{\int_{-\infty}^{\infty} d\xi |\hat{a}|^2}, \quad (\text{B20})$$

$$\zeta_G = \frac{\int_0^{\infty} dr r \int_{-\infty}^{\infty} d\xi \xi |\hat{a}|^2}{\int_0^{\infty} dr r \int_{-\infty}^{\infty} d\xi |\hat{a}|^2}. \quad (\text{B21})$$

The local pulse centroid is given by  $\zeta_L = -\psi_i'$ . The axial group velocity associated with the local centroid  $v_L$  is defined by  $d\zeta_L/dt = v_L - v_{g0}$ , i.e.,

$$v_L \approx v_{g0} \left\{ 1 + \frac{2}{k_0^2 r_0^2} \left[ \frac{(3\alpha_0^2 + \alpha_0^4)}{(1+\alpha_0^2)^2} + \frac{(1-6\alpha_0^2 + \alpha_0^4)r^2}{(1+\alpha_0^2)^3 r_0^2} \right] \right\}. \quad (\text{B22})$$

In general, the local centroid velocity  $v_L = v_L(r, z)$  is a function of both  $r$  and  $z$ . However,  $v_L = v_{g0}$  at  $z=0$  and  $r=0$ . Hence, the value of  $v_{g0} = c\beta_{g0}$  given by  $\beta_{g0}^2 = 1 - \omega_{p0}^2/\omega_0^2 - 4c^2/\omega_0^2 r_0^2$  is the correct value of the group velocity of the local pulse centroid at the focal point to first order in  $\delta k/k_0$ . As the pulse diffracts, the local centroid velocity slightly increases. Asymptotically, for  $z/Z_{R0} \gg 1$  and  $r=0$ ,  $v_L \approx v_{g0}(1 + 2/k_0^2 r_0^2) \approx 1 - \omega_{p0}^2/2\omega_0^2$ , which is the 1D value.

Inserting Eq. (B17) into Eq. (B21), the global centroid is given by  $\zeta_G \approx \alpha_0/2k_0$ . The axial group velocity associated with the global centroid  $v_G$ , defined by  $d\zeta_G/dt = v_G - v_{g0}$ , is given by

$$v_G \approx v_{g0}(1 + 1/k_0^2 r_0^2) \approx c(1 - \omega_{p0}^2/2\omega_0^2 - 1/k_0^2 r_0^2), \quad (\text{B23})$$

plus corrections of order  $(k_0^2 r_0 L)^{-2}$  or higher. Hence, for the entire pulse, the global centroid velocity  $v_G$ , Eq. (B23), is constant (independent of  $z$ ) and slightly higher ( $v_G > v_{g0}$ ) than the value of the local centroid velocity at the focal point  $v_L(0,0) = v_{g0}$ . The velocities of the local and global pulse centroids given by Eqs. (B22) and (B23) have been confirmed by numerical solutions of the wave equation [41].

### 3. Second-order solution

To second order,  $\hat{a}_k = b_{k0} \exp(\psi + \psi' \delta k + \psi'' \delta k^2/2)$ . The inverse transform of this can be readily obtained for a Gaussian axial profile,  $b_{k0} = (a_0 L/\sqrt{2}) \exp(-\delta k^2 L^2/4)$ , i.e.,

$$\hat{a} = a_0 \left( 1 - \frac{2\psi''}{L^2} \right)^{-1/2} \exp \left[ \psi - \frac{(\zeta - i\psi')^2/L^2}{(1 - 2\psi''/L^2)} \right]. \quad (\text{B24})$$

Note that the validity of the expansion given by Eq. (B10) implies that  $|2\psi''/L^2| \ll 1$ .

### APPENDIX C: HIGHER-ORDER MODES

In this appendix, the results of Sec. II are generalized to include higher-order modes. In analogy with Eq. (9), consider the wave equation describing the evolution of the Fourier transform of the pulse envelope  $\hat{a}_k$ ,

$$\left( \nabla_{\perp}^2 + 2ik \frac{\partial}{\partial z} \right) \hat{a}_k = [k_p^2(r) - k_0^2(\beta_{p0}^2 - 1) + \delta k^2(1 - \beta_{g0}^2)] \hat{a}_k, \quad (\text{C1})$$

where  $k = k_0 + \delta k$ , the  $\partial^2/\partial z^2$  term has been neglected in the wave operator, and a parabolic density channel will be assumed  $k_p^2 = k_{p0}^2(1 + \Delta n r^2/n_0 r_0^2)$ . A general solution to Eq. (C1) is a Laguerre-Gaussian mode, characterized by the mode numbers  $m$  and  $p$ , of the form

$$\hat{a}_k = b_k s^{p/2} L_m^p(s) \exp[i\theta - (1 - i\alpha)s/2 + ip\phi], \quad (\text{C2})$$

where  $s = 2r^2/r_s^2$ ,  $L_m^p$  is the generalized Laguerre polynomial, and  $\phi$  is the polar angular coordinate (axisymmetric modes correspond to  $p=0$ ). By inserting Eq. (C2) into Eq. (C1), it can be shown that the functions  $b_k(z)$ ,  $r_s(z)$ ,  $\alpha(z)$ , and  $\theta(z)$  satisfy

$$b_k = b_{k0} r_s / r_0, \quad (\text{C3})$$

$$\alpha = (kr_s/2) \partial r_s / \partial z, \quad (\text{C4})$$

$$\frac{\partial^2 r_s}{\partial z^2} = \frac{4}{k^2 r_s^3} \left( 1 - \frac{\Delta n r_s^4}{\Delta n_c r_0^4} \right), \quad (\text{C5})$$

$$\frac{\partial \theta}{\partial z} = -\frac{1}{2k} \left[ \frac{4}{r_s^2} (2m + p + 1) + k_{p0}^2 - k_0^2(\beta_{p0}^2 - 1) + \delta k^2(1 - \beta_{g0}^2) \right], \quad (\text{C6})$$

where  $k = k_0 + \delta k$ ,  $\Delta n_c = 1/\pi r_e r_0^2$  is the critical channel depth, and  $b_{k0}$  is the initial  $\delta k$  spectrum of the laser pulse at  $z=0$ .

The quantities  $b_k$ ,  $\alpha$ , and  $r_s$  are independent of the mode numbers  $m$  and  $p$  and identical to the previous results, Eqs. (12a)–(12c). Hence, the condition for a matched pulse ( $r_s = r_0$  for  $\Delta n = \Delta n_c$ ) is the same for all modes. The quantity  $\theta$ , however, does depend on  $m$  and  $p$  as well as on the choice of  $\beta_{g0}$  ( $\beta_{g0}\beta_{p0} = 1$ ). For consistency, the previous choice for  $\beta_{g0} = ck_0/\omega_0$  will be used, i.e.,  $1 - \beta_{g0}^2 = \omega_{p0}^2/\omega_0^2 + 4c^2/\omega_0^2 r_0^2$ , such that  $k_{p0}^2 - k_0^2(\beta_{p0}^2 - 1) = -4/r_0^2$ . Note that this choice for  $\beta_{g0}$  gives the correct axial group velocity for matched propagation ( $r_s = r_0$ ) of the fundamental ( $m=p=0$ ) mode. For the higher-order modes, however, it can be

shown that the axial group velocity of a matched mode is given by  $\beta_g$ , where

$$1 - \beta_g^2 \approx \omega_{p0}^2/\omega_0^2 + 4(2m+p+1)c^2/\omega_0^2 r_0^2. \quad (C7)$$

The correct value for the axial group velocity is manifested in the value of the effective axial wave-number shift (relative to the fundamental),  $\Delta k_z \approx \partial\theta/\partial z$ , evaluated in the paraxial limit ( $\delta k=0$ ) for a matched laser pulse ( $r_s=r_0$ ), i.e.,  $\beta_g \approx c(k_0 + \Delta k_z)/\omega_0 \approx \beta_{g0}(1 + \Delta k_z/k_0)$ , where  $\Delta k_z \approx -2(2m+p)/k_0 r_0^2$ .

For propagation in a parabolic channel ( $\Delta n > 0$ ), the solutions to Eqs. (C4)–(C6) with the initial (at  $z=0$ ) conditions  $\alpha=0$ ,  $\theta=0$ ,  $\partial r_s/\partial z=0$ , and  $r_s=r_i$  are given by

$$\alpha = -\frac{1}{2} \left( \frac{r_i^2}{r_M^2} - \frac{r_M^2}{r_i^2} \right) \sin(k_\beta z), \quad (C8)$$

$$r_s^2 = \frac{r_i^2}{2} \left[ \left( 1 + \frac{r_M^4}{r_i^4} \right) + \left( 1 - \frac{r_M^4}{r_i^4} \right) \cos(k_\beta z) \right], \quad (C9)$$

$$\theta = \left[ \frac{r_M^2}{r_0^2} - \frac{\delta k^2 r_M^2}{4} (1 - \beta_{g0}^2) \right] \frac{z}{Z_{RM}} - (2m+p+1) \tan^{-1} \left[ \frac{r_M^2}{r_i^2} \tan \left( \frac{z}{Z_{RM}} \right) \right], \quad (C10)$$

where  $k_\beta = 2/Z_{RM}$  is the betatron wave number,  $Z_{RM} = kr_M^2/2$  is the matched Rayleigh length, and  $r_M = (r_0^4 \Delta n_c / \Delta n)^{1/4}$  is the matched spot size ( $r_M=r_0$  for  $\Delta n = \Delta n_c$ ). For a matched pulse,  $r_s=r_i=r_M$ ,  $\alpha=0$ , and  $\theta = -(2m+p)k_\beta z/2 - \delta k^2(1 - \beta_{g0}^2)z/2k$ .

For propagation in vacuum ( $\Delta n=0$ ), the solution to Eqs. (C4)–(C6) for the initial ( $z=0$ ) conditions  $r_s=r_0$ ,  $dr_s/dz=0$ ,  $\alpha=0$ , and  $\theta=0$  are given by

$$\alpha = z/Z_R, \quad (C11)$$

$$r_s = r_0(1 + \alpha^2)^{1/2}, \quad (C12)$$

$$\theta = \alpha - (2m+p+1) \tan^{-1} \alpha - (\delta k^2 r_0^2/4)(1 - \beta_{g0}^2)\alpha, \quad (C13)$$

where  $Z_R = kr_0^2/2$  and  $r_0$  is the minimum spot size at the focal point (assumed to be at  $z=0$ ).

- 
- [1] For a review, see E. Esarey, P. Sprangle, J. Krall, and A. Ting, IEEE J. Quantum Electron. **33**, 1879 (1997).
- [2] For a review, see E. Esarey, P. Sprangle, J. Krall, and A. Ting, IEEE Trans. Plasma Sci. **24**, 252 (1996); W. P. Leemans, C. W. Siders, E. Esarey, N. Andreev, G. Shvets, and W. B. Mori, *ibid.* **24**, 331 (1996).
- [3] H. M. Milchberg, C. G. Durfee III, and T. J. MacIlrath, Phys. Rev. Lett. **75**, 2494 (1995).
- [4] C. G. Durfee, S. Backus, M. M. Murnane, and H. C. Kapteyn, Opt. Lett. **22**, 1565 (1997).
- [5] D. C. Eder, P. Amemdt, L. B. DaSilva, R. A. London, B. J. MacGowan, D. L. Matthews, B. M. Penetrqante, M. D. Rosen, S. C. Wilks, T. D. Donnelly, R. W. Falcone, and G. L. Strobel, Phys. Plasmas **1**, 1744 (1994).
- [6] S. Suckewer and C. H. Skinner, Comments At. Mol. Phys. **30**, 331 (1995).
- [7] M. Tabak, J. Hammer, M. E. Glinsky, W. L. Kruer, S. C. Wilks, J. Woodworth, E. M. Campbell, M. D. Perry, and R. J. Mason, Phys. Plasmas **1**, 1626 (1994).
- [8] C. Deutsch, H. Furukawa, K. Mima, M. Murakami, and K. Nishihara, Phys. Rev. Lett. **77**, 2483 (1996).
- [9] A. Pukhov and J. Meyerter-Vehn, Phys. Rev. Lett. **79**, 2686 (1997).
- [10] P. Sprangle and E. Esarey, Phys. Fluids B **4**, 2241 (1992).
- [11] P. Sprangle, E. Esarey, J. Krall, and G. Joyce, Phys. Rev. Lett. **69**, 2200 (1992).
- [12] C. G. Durfee and H. M. Milchberg, Phys. Rev. Lett. **71**, 2409 (1993).
- [13] C. G. Durfee, J. Lynch, and H. M. Milchberg, Phys. Rev. E **51**, 2368 (1995).
- [14] H. M. Milchberg, T. R. Clark, C. G. Durfee, T. M. Antonsen, and P. Mora, Phys. Plasmas **3**, 2149 (1996).
- [15] T. R. Clark and H. M. Milchberg, Phys. Rev. Lett. **78**, 2373 (1997).
- [16] S. P. Nikitin, T. M. Antonsen, T. R. Clark, Y. L. Li, and H. M. Milchberg, Opt. Lett. **22**, 1787 (1997).
- [17] T. Ditmire, R. A. Smith, and M. H. R. Hutchinson, Opt. Lett. **23**, 322 (1998).
- [18] W. P. Leemans, P. Volfbeyn, K. Z. Guo, S. Chattopadhyay, C. B. Schroeder, B. A. Shadwick, P. B. Lee, J. S. Wurtele, and E. Esarey, Phys. Plasmas **5**, 1615 (1998).
- [19] A. Zigler, Y. Ehrlich, C. Cohen, J. Krall, and P. Sprangle, J. Opt. Soc. Am. B **13**, 68 (1996).
- [20] Y. Ehrlich, C. Cohen, A. Zigler, J. Krall, P. Sprangle, and E. Esarey, Phys. Rev. Lett. **77**, 4186 (1996).
- [21] Y. Ehrlich, C. Cohen, D. Kaganovich, A. Zigler, R. F. Hubbard, P. Sprangle, and E. Esarey, J. Opt. Soc. Am. B **15**, 2416 (1998); R. F. Hubbard, in Advanced Accelerator Concepts, edited by W. Lawson, AIP Conf. Proc. (AIP, NY, in press).
- [22] K. Krushelnick, A. Ting, C. I. Moore, H. R. Burris, E. Esarey, P. Sprangle, and M. Baine, Phys. Rev. Lett. **78**, 4047 (1997).
- [23] A. Ting, C. I. Moore, K. Krushelnick, C. Manka, E. Esarey, P. Sprangle, R. Hubbard, H. R. Burris, and M. Baine, Phys. Plasmas **4**, 1889 (1997).
- [24] S. Y. Chen, G. S. Sarkisov, A. Maksimchuk, R. Wagner, and D. Umstadter, Phys. Rev. Lett. **80**, 2610 (1998).
- [25] A. B. Borisov, X. Shi, V. B. Karpov, V. V. Korobkin, J. C. Solem, O. B. Shiryayev, A. McPherson, K. Boyer, and C. K. Rhodes, J. Opt. Soc. Am. B **11**, 1941 (1994).
- [26] P. Gibbon, F. Jakober, P. Monet, and T. Auguste, IEEE Trans. Plasma Sci. **24**, 343 (1996).
- [27] A. Chiron, G. Bonnaud, A. Dulieu, J. L. Miquel, G. Malka, and M. Louis-Jacquet, Phys. Plasmas **3**, 1373 (1996).
- [28] P. E. Young and P. R. Bolton, Phys. Rev. Lett. **77**, 4556 (1996).

- [29] M. Borghesi, A. J. MacKinnon, L. Barringer, R. Gaillard, L. A. Gizzi, C. Meyer, O. Willi, A. Pukhov, and J. Meyer-ter-Vehn, *Phys. Rev. Lett.* **78**, 879 (1997).
- [30] J. Fuchs, G. Malka, J. C. Adam, F. Amiranoff, S. D. Baton, N. Blanchot, A. Heron, G. Laval, J. L. Miquel, P. Mora, H. Pepin, and C. Rousseaux, *Phys. Rev. Lett.* **80**, 1658 (1998).
- [31] C. E. Clayton, K. C. Tzeng, D. Gordon, P. Muggli, W. B. Mori, C. Joshi, V. Malka, Z. Najmudin, A. Modena, and A. E. Dangor, *Phys. Rev. Lett.* **81**, 100 (1998).
- [32] G. A. Mourou, C. P. J. Barty, and M. D. Perry, *Phys. Today* **51**(1), 22 (1998).
- [33] E. Esarey, J. Krall, and P. Sprangle, *Phys. Rev. Lett.* **72**, 2887 (1994).
- [34] P. Sprangle, C. M. Tang, and E. Esarey, *IEEE Trans. Plasma Sci.* **15**, 145 (1987).
- [35] G. Z. Sun, E. Ott, Y. C. Lee, and P. Guzdar, *Phys. Fluids* **30**, 526 (1987).
- [36] P. Sprangle, E. Esarey, and A. Ting, *Phys. Rev. Lett.* **64**, 2011 (1990); *Phys. Rev. A* **41**, 4463 (1990).
- [37] A. B. Borisov, A. V. Borovskiy, O. B. Shiryaev, V. V. Korobkin, A. M. Prokhorov, J. C. Solem, T. S. Luk, K. Boyer, and C. K. Rhodes, *Phys. Rev. A* **45**, 5830 (1992).
- [38] H. S. Brandi, C. Manus, G. Mainfray, T. Lehner, and G. Bonnaud, *Phys. Fluids B* **5**, 3539 (1993); G. Bonnaud, H. S. Brandi, C. Manus, G. Mainfray, and T. Lehner, *Phys. Plasmas* **1**, 968 (1994).
- [39] T. C. Chiou, T. Katsouleas, C. Decker, W. B. Mori, J. S. Wurtele, G. Shvets, and J. J. Su, *Phys. Plasmas* **2**, 310 (1995).
- [40] P. Volfbeyn, P. B. Lee, J. Wurtele, W. P. Leemans, and G. Shvets, *Phys. Plasmas* **4**, 3403 (1997).
- [41] E. Esarey, P. Sprangle, M. Pilloff, and J. Krall, *J. Opt. Soc. Am. B* **12**, 1695 (1995).
- [42] T. M. Antonsen, Jr. and P. Mora, *Phys. Rev. Lett.* **69**, 2204 (1992); *Phys. Fluids B* **5**, 1440 (1993).
- [43] N. E. Andreev, V. I. Kirsanov, and L. M. Gorbunov, *Phys. Plasmas* **2**, 2573 (1995); N. E. Andreev, V. I. Kirsanov, L. M. Gorbunov, and A. S. Sakharov, *IEEE Trans. Plasma Sci.* **24**, 363 (1996).
- [44] W. B. Mori, C. D. Decker, D. E. Hinkel, and T. Katsouleas, *Phys. Rev. Lett.* **72**, 1482 (1994); C. D. Decker, W. B. Mori, T. Katsouleas, and D. E. Hinkel, *Phys. Plasmas* **3**, 1360 (1996).
- [45] G. Shvets and J. S. Wurtele, *Phys. Rev. Lett.* **73**, 3540 (1994).
- [46] P. Sprangle, J. Krall, and E. Esarey, *Phys. Rev. Lett.* **73**, 3544 (1994).
- [47] G. P. Agrawal, *Nonlinear Fiber Optics* (Academic, New York, 1995).
- [48] T. M. Antonsen and P. Mora, *Phys. Rev. Lett.* **74**, 4440 (1995).